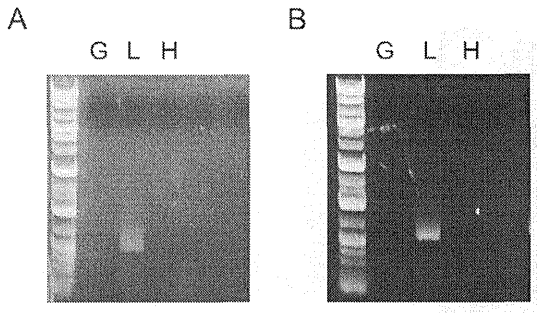

Figure 5. Reverse transcription-PCR for endogenous HNF1α and HNF1β in wild-type pigs at 4 weeks of age. Both HNF1α (**A**) and HNF1β (**B**) were negative in isolated glomeruli. Liver was used as a positive control, and heart as a negative control. G = isolated glomeruli; L = liver; H = heart.
doi:10.1371/journal.pone.0092219.g005

cellular response in these species is different under diabetic conditions. Several reports of nodular sclerosis in the diabetic rodent model support this explanation.

In addition to the mesangial changes under hyperglycemia, our model suggests the involvement of unique hemodynamic factors in nodular morphogenesis. Glomerular hyperfiltration or hypertrophy promotes diabetic nephropathy; however, whether glomerular hemodynamic effects accelerate the formation of diabetic nodules in humans remains controversial. Accordingly, the present study showed that glomerular nodular lesions in diabetic pigs were localized predominantly in the deep cortex. Notably, glomeruli were significantly larger in the deep cortex of diabetic pigs compared to in that of wild-type pigs, but were unchanged in the superficial cortex of both groups. These observations suggest that glomerular hemodynamic effects also promote formation of glomerular nodular lesions in diabetic pigs. Similarly, diabetic nephropathy was accelerated in eNOS-knockout mice, attenuated by improvement of eNOS activity in *db/db* mice [32,33], and antihypertensive therapy alone significantly suppressed the development of nodular lesions and mesangiolysis in diabetic eNOS-knockout mice [34]. Based on these reports and our current findings, our results suggest the involvement of glomerular hypertension in nodular lesion formation in diabetes. Therefore, prominent glomerular hyperfiltration and hypertrophy may be the basis of glomerular nodule development in our diabetic pig model.

The inserted dominant-negative human MODY gene might have stimulated mesangial matrix synthesis by inhibiting endogenous HNF1α or HNF1β function, regardless of the diabetic milieu. Typically, HNF1α functions as a homodimer or a heterodimer with the structurally related protein HNF1β [14,15,35]. Thus, a dominant-negative mutant HNF1αP291fsinsC should inhibit HNF1α or HNF1β by forming an inactive heterodimer at the site of endogenous HNF1α or HNF1β expression. The RT-PCR study confirmed that mutant HNF1αP291fsinsC could not interact with endogenous HNF1α and HNF1β in the glomeruli of transgenic pigs. This supports the notion that the diabetic milieu, but not the genetic alteration, promotes glomerular nodular formation in the pig model.

Our diabetic pig model lacks several diabetic renal features characteristic of human diabetic nephropathy; e.g., proteinuria, GBM thickening, exudative lesions, tubular atrophy, interstitial fibrosis and arteriolar hyalinosis. Furthermore, the glomeruli did not undergo glomerulosclerosis. These results suggest that our model does not accurately reproduce human diabetic nephropathy, even in pigs carrying the human MODY3 gene. In addition to the species difference in the cellular response to hyperglycemia, a possible explanation for this discrepancy is that we were unable to monitor the histology for a sufficiently long period because due to the relatively short lifespan of the pigs. In addition, the mechanism of nodular formation is considered to be different from that of other diabetic kidney lesions. Nevertheless, this pig model indicated that glomerular nodules could form independently of diabetic complications.

In conclusion, this was the first report of distinct and reproducible glomerular nodular lesions in transgenic pigs carrying a dominant-negative HNF1α mutation of the human MODY3 gene. Although there were several differences compared to the pathology of human glomerular nodular lesions, the somewhat acute and constitutive formation of nodules in the mammalian models might provide information that will facilitate identification of the principal mechanism underlying glomerular nodular formation.

Supporting Information

Figure S1 Body weight and diabetic parameter changes over time. A) Body weight was lower in transgenic pigs than in wild-type pigs. **B**) Plasma glucose was at a high level in transgenic pigs. **C**) 1,5-Anhydroglucitol was at a low level in transgenic pigs. Tg = transgenic pigs (n = 1); WT = wild-type pigs (up to 6 months of age, n = 3; 6–10 months of age, n = 1).
(TIF)

Figure S2 Armanni-Ebstein lesions in diabetic pigs at 19 weeks of age. Transgenic pigs revealed vacuolation of proximal tubules known as Armanni-Ebstein lesions. Note that distal tubules and the collecting duct are intact. **A**) Magnification: 100×. **B**) Magnification: 400×.
(TIF)

Author Contributions

Conceived and designed the experiments: KU HN. Performed the experiments: KU TY SH. Analyzed the data: SH TY MN. Contributed reagents/materials/analysis tools: SH TY KU HN MN. Wrote the paper: SH KU MN.

References

1. Nakai S, Iseki K, Itami N, Ogata S, Kazama JJ, et al. (2012) An overview of regular dialysis treatment in Japan (as of 31 December 2010). Ther Apher Dial 16: 483–521.
2. White SL, Chadban SJ, Jan S, Chapman JR, Cass A (2008) How can we achieve equity in provision of renal replacement therapy? Bull World Health Organ 86: 229–237.
3. Kimmelstiel P, Wilson C (1936) Intercapillary Lesions in the Glomeruli of the Kidney. Am J Pathol 12: 83–98.7.
4. Hong D, Zheng T, Jia-qing S, Jian W, Zhi-hong L, et al. (2007) Nodular glomerular lesion: a later stage of diabetic nephropathy? Diabetes Res Clin Pract 78: 189–195.
5. Heaf JG, Løkkegaard H, Larsen S (2001) The relative prognosis of nodular and diffuse diabetic nephropathy. Scand J Urol Nephrol 35: 233–238.
6. Brosius FC 3rd, Alpers CE, Bottinger EP, Breyer MD, Coffman TM, et al. (2009) Mouse models of diabetic nephropathy. J Am Soc Nephrol 20: 2503–2512.
7. Zhao HJ, Wang S, Cheng H, Zhang MZ, Takahashi T, et al. (2006) Endothelial nitric oxide synthase deficiency produces accelerated nephropathy in diabetic mice. J Am Soc Nephrol 17: 2664–2669.
8. Inagi R, Yamamoto Y, Nangaku M, Usuda N, Okamoto H, et al. (2006) A severe diabetic nephropathy model with early development of nodule-like lesions induced by megsin overexpression in RAGE/iNOS transgenic mice. Diabetes 55: 356–366.

9. Furuichi K, Hisada Y, Shimizu M, Okumura T, Kitagawa K, et al. (2011) Matrix metalloproteinase-2 (MMP-2) and membrane-type 1 MMP (MT1-MMP) affect the remodeling of glomerulosclerosis in diabetic OLETF rats. Nephrol Dial Transplant 26: 3124–3131.
10. Hudkins KL, Pichaiwong W, Wietecha T, Kowalewska J, Banas M, et al. (2010) BTBR ob/ob mutant mice model progressive diabetic nephropathy. J Am Soc Nephrol 21: 1533–1542.
11. Larsen MO, Wilken M, Gotfredsen CF, Carr RD, Svendsen O, et al. (2002) Mild streptozotocin diabetes in the Göttingen minipig. A novel model of moderate insulin deficiency and diabetes. Am J Physiol Endocrinol Metab 282: E1342–1351.
12. Bellinger DA, Merricks EP, Nichols TC (2006) Swine models of type 2 diabetes mellitus: insulin resistance, glucose tolerance, and cardiovascular complications. ILAR J 47: 243–258.
13. Renner S, Braun-Reichhart C, Blutke A, Herbach N, Emrich D, et al. (2013) Permanent neonatal diabetes in INS(C94Y) transgenic pigs. Diabetes 62: 1505–1511.
14. Yamagata K, Oda N, Kaisaki PJ, Menzel S, Furuta H, et al. (1996) Mutations in the hepatocyte nuclear factor-1α gene in maturity-onset diabetes of the young (MODY3). Nature 384: 455–458.
15. Yamagata K (2003) Regulation of pancreatic β-cell function by the HNF transcription network: lessons from maturity-onset diabetes of the young (MODY). Endocr J 50: 491–499.
16. Pontoglio M, Barra J, Hadchouel M, Doyen A, Kress C, et al. (1996) Hepatocyte nuclear factor 1 inactivation results in hepatic dysfunction, phenylketonuria, and renal Fanconi syndrome. Cell 84: 575–585.
17. Pontoglio M (2000) Hepatocyte nuclear factor 1, a transcription factor at the crossroads of glucose homeostasis. J Am Soc Nephrol 11: S140–S143.
18. Umeyama K, Watanabe M, Saito H, Kurome M, Tohi S, et al. (2009) Dominant-negative mutant hepatocyte nuclear factor 1alpha induces diabetes in transgenic-cloned pigs. Transgenic Res 18: 697–706.
19. Umeyama K, Honda K, Matsunari H, Nakano K, Hidaka T, et al. (2013) Production of diabetic offspring using cryopreserved epididymal sperm by in vitro fertilization and intrafallopian insemination techniques in transgenic pigs. J Reprod Dev 59: 599–603.
20. Tanji N, Markowitz GS, Fu C, Kislinger T, Taguchi A, et al. (2000) Expression of advanced glycation end products and their cellular receptor RAGE in diabetic nephropathy and nondiabetic renal disease. J Am Soc Nephrol 11: 1656–1666.
21. Horie K, Miyata T, Maeda K, Miyata S, Sugiyama S, et al. (1997) Immunohistochemical colocalization of glycoxidation products and lipid peroxidation products in diabetic renal glomerular lesions. Implication for glycoxidative stress in the pathogenesis of diabetic nephropathy. J Clin Invest 100: 2995–3004.
22. Yamamoto T, Nakamura T, Noble NA, Ruoslahti E, Border WA (1993) Expression of transforming growth factor beta is elevated in human and experimental diabetic nephropathy. Proc Natl Acad Sci U S A 90: 1814–1818.
23. Ritchie S, Waugh D (1957) The pathology of Armanni-Ebstein diabetic nephropathy. Am J Pathol 33: 1035–1057.
24. Nerlich A, Schleicher E (1991) Immunohistochemical localization of extracellular matrix components in human diabetic glomerular lesions. Am J Pathol 139: 889–899.
25. Makino H, Shikata K, Wieslander J, Wada J, Kashihara N, et al. (1994) Localization of fibril/microfibril and basement membrane collagens in diabetic glomerulosclerosis in type 2 diabetes. Diabet Med 11: 304–311.
26. Glick AD, Jacobson HR, Haralson MA (1992) Mesangial deposition of type I collagen in human glomerulosclerosis. Hum Pathol 23: 1373–1379.
27. Renner S, Braun-Reichhart C, Blutke A, Herbach N, Emrich D, et al. (2001) Biochemistry and molecular cell biology of diabetic complications. Nature 414: 813–820.
28. Yamagishi S, Matsui T (2010) Advanced glycation end products, oxidative stress and diabetic nephropathy. Oxid Med Cell Longev 3: 101–108.
29. Fukami K, Ueda S, Yamagishi S, Kato S, Inagaki Y, et al. (2004) AGEs activate mesangial TGF-β-Smad signaling via an angiotensin II type I receptor interaction. Kidney Int 66: 2137–2147.
30. Mason RM, Wahab NA (2003) Extracellular matrix metabolism in diabetic nephropathy. J Am Soc Nephrol 14: 1358–1373.
31. Yan SD, Schmidt AM, Anderson GM, Zhang J, Brett J, et al. (1994) Enhanced cellular oxidant stress by the interaction of advanced glycation end products with their receptors/binding proteins. J Biol Chem 269: 9889–9897.
32. Kanetsuna Y, Takahashi K, Nagata M, Gannon MA, Breyer MD, et al. (2007) Deficiency of endothelial nitric-oxide synthase confers susceptibility to diabetic nephropathy in nephropathy-resistant inbred mice. Am J Pathol 170: 1473–1484.
33. Cheng H, Wang H, Fan X, Paueksakon P, Harris RC (2012) Improvement of endothelial nitric oxide synthase activity retards the progression of diabetic nephropathy in db/db mice. Kidney Int 82: 1176–1183.
34. Kosugi T, Heinig M, Nakayama T, Connor T, Yuzawa Y, et al. (2009) Lowering blood pressure blocks mesangiolysis and mesangial nodules, but not tubulointerstitial injury, in diabetic eNOS knockout mice. Am J Pathol 174: 1221–1229.
35. Mendel DB, Hansen LP, Graves MK, Conley PB, Crabtree GR (1991) HNF-1 alpha and HNF-1 beta (vHNF-1) share dimerization and homeo domains, but not activation domains, and form heterodimers in vitro. Genes Dev 5: 1042–1056.

PLOS ONE

Generation of Interleukin-2 Receptor Gamma Gene Knockout Pigs from Somatic Cells Genetically Modified by Zinc Finger Nuclease-Encoding mRNA

Masahito Watanabe[1,2], Kazuaki Nakano[1], Hitomi Matsunari[1,2], Taisuke Matsuda[1], Miki Maehara[1], Takahiro Kanai[1], Mirina Kobayashi[1], Yukina Matsumura[1], Rieko Sakai[1], Momoko Kuramoto[1], Gota Hayashida[1], Yoshinori Asano[1], Shuko Takayanagi[1], Yoshikazu Arai[1], Kazuhiro Umeyama[1,2], Masaki Nagaya[2], Yutaka Hanazono[3,4], Hiroshi Nagashima[1,2,4]*

1 Laboratory of Developmental Engineering, Department of Life Sciences, School of Agriculture, Meiji University, Kawasaki, Japan, **2** Meiji University International Institute for Bio-Resource Research (MUIIBR), Kawasaki, Japan, **3** Division of Regenerative Medicine, Center for Molecular Medicine, Jichi Medical University, Tochigi, Japan, **4** CREST, Japan Science and Technology Agency, Tokyo, Japan

Abstract

Zinc finger nuclease (ZFN) is a powerful tool for genome editing. ZFN-encoding plasmid DNA expression systems have been recently employed for the generation of gene knockout (KO) pigs, although one major limitation of this technology is the use of potentially harmful genome-integrating plasmid DNAs. Here we describe a simple, non-integrating strategy for generating KO pigs using ZFN-encoding mRNA. The interleukin-2 receptor gamma (*IL2RG*) gene was knocked out in porcine fetal fibroblasts using ZFN-encoding mRNAs, and *IL2RG* KO pigs were subsequently generated using these KO cells through somatic cell nuclear transfer (SCNT). The resulting *IL2RG* KO pigs completely lacked a thymus and were deficient in T and NK cells, similar to human X-linked SCID patients. Our findings demonstrate that the combination of ZFN-encoding mRNAs and SCNT provides a simple robust method for producing KO pigs without genomic integration.

Citation: Watanabe M, Nakano K, Matsunari H, Matsuda T, Maehara M, et al. (2013) Generation of Interleukin-2 Receptor Gamma Gene Knockout Pigs from Somatic Cells Genetically Modified by Zinc Finger Nuclease-Encoding mRNA. PLoS ONE 8(10): e76478. doi:10.1371/journal.pone.0076478

Editor: Andrew C. Wilber, Southern Illinois University School of Medicine, United States of America

Received July 4, 2013; **Accepted** August 23, 2013; **Published** October 9, 2013

Funding: This work was supported by the Core Research for Evolutional Science and Technology (CREST) of the Japan Science and Technology Agency and by the Meiji University International Institute for Bio-Resource Research (MUIIBR). The funders had no role in study design, data collection and analysis, decision to publish, or preparation of the manuscript.

Competing Interests: The authors have declared that no competing interests exist.

* E-mail: hnagas@isc.meiji.ac.jp

Introduction

Pigs have attracted attention as large experimental animals capable of providing valuable information that is highly extrapolatable to humans due to their anatomical, physiological, and hematological features [1–5]. To date, pig models of various human diseases, such as cystic fibrosis [6], diabetes mellitus [7,8], Alzheimer's disease [9], and retinitis pigmentosa [10], have been created. In addition, research on the use of genetically modified pigs as organ/tissue donors for xenotransplantation into humans is advancing [11,12]. In fact, encapsulated porcine islets of Langerhans have been transplanted into humans and are now under clinical trials to assess their safety and efficacy for curing type I diabetes mellitus [13].

The knockout (KO) of endogenous genes is a useful tool for analyses of gene function and the production of animal models that mimic human diseases. A variety of gene KO mice have been generated using embryonic stem (ES) cells genetically modified by homologous recombination (HR). As authentic ES cells are not available in pigs, HR using somatic cells has been employed to generate gene KO pigs in combination with somatic cell nuclear transfer (SCNT) technology. However, the low efficiency (frequency, 10^{-6} to 10^{-8}) of HR for mammalian cultured cells hinders the generation of KO pigs [14–16], and the generation of KO pigs through HR therefore remains limited.

One new technique uses zinc finger nucleases (ZFNs) to knock out endogenous genes and is expected to overcome the inefficiency and complexity of HR in mammals [17]. Engineered ZFNs are artificial restriction enzymes comprised of a zinc finger DNA-binding domain and a DNA cleavage domain [18]. We previously were the first to demonstrate that gene KO in primary porcine fetal fibroblasts *in vitro* was possible using ZFNs [19], and somatic cells that were genetically modified by ZFNs were shown to be capable of producing gene KO pigs after SCNT [20–23]. In these studies, the ZFN-encoding plasmid DNA was introduced into somatic cells or the nuclear donor cells for SCNT. However, plasmid DNA can also be integrated into the genome of cells, which may result in the disruption of endogenous genes and the constitutive expression of ZFNs. This drawback of plasmid DNA can be eliminated by the use of ZFN-encoding mRNA, which cannot be inserted into the host genome. Gene KO using ZFN-encoding mRNAs in rodents has been performed via direct injection into the fertilized eggs [24–26], although the generation of KO piglets using ZFN-encoding mRNA has yet to be reported.

The present study sought to investigate whether ZFN-encoding mRNAs can be used to generate gene KO pigs. We chose the

interleukin-2 receptor gamma (*IL2RG*) gene on the X-chromosome of male cells as a target gene to be knocked out. *IL2RG* encodes the common gamma chain (γ_c), and mutations in *IL2RG* lead to X-linked severe combined immunodeficiency (XSCID), which is characterized by profound defects in cellular and humoral immunity in humans [27,28]. Furthermore, knockout of *IL2RG* was previously shown to give rise to the XSCID phenotype in male pigs [29]. We therefore applied ZFN-encoding mRNA to knock out *IL2RG* in male porcine fibroblast cells, which are capable of supporting the development to live offspring after SCNT. Here, we show that an endogenous gene in porcine primary cultured cells could be knocked out using ZFN-encoding mRNAs, thereby allowing the efficient production of a gene KO pig by means of somatic cell cloning.

Results

Design of ZFNs and isolation of *IL2RG* KO cells

Similar to *IL2RG* in humans, mice, and rats, porcine *IL2RG* is found on the X chromosome and consists of 8 exons [30]. In this study, we constructed a ZFN that targets exon 1 of porcine *IL2RG*. This pair (right and left) of ZFNs contains 4 zinc finger proteins each, and both the right and left ZFNs recognize a target sequence of 24 bp (Figure 1A). *IL2RG* KO cells were generated via the electroporation of ZFN-encoding mRNAs into porcine male fetal fibroblasts with transient cold shock treatment at 32°C for 3 d [31]. No visible morphological abnormalities were detected in the fetal fibroblasts following the introduction of mRNA and transient cold shock treatment. Of the 192 single cell-derived cell lines obtained by limiting dilution, 1 cell line (1/192, 0.5%) with a ZFN-induced mutation was established, and this cell line (#98, Figure 1B) was used as the nuclear donor for SCNT. DNA sequence analyses showed that these cells carried both a 3-bp substitution and an 86-bp deletion spanning the major transcription start point and the start codon (ATG) of porcine *IL2RG*, indicating that this mutation was likely to disrupt *IL2RG* function. Sufficient numbers of KO cells were prepared for SCNT after culture for 3 weeks.

Production and analysis of *IL2RG* KO cloned pigs

First, the developmental competence of the SCNT embryos reconstructed with the *IL2RG* KO cells was examined *in vitro*. Of the 403 SCNT embryos produced in duplicated experiments, 237 (58.8%) developed into blastocysts (Table 1). This blastocyst formation rate was comparable to those reported in our previous studies [32]. Second, 199 blastocysts (Figure 2A) obtained by SCNT were subjected to transfer to 2 estrus synchronized recipient gilts (P177 and P178; Table 1). Pregnancy was confirmed in both gilts at 39 d of gestation. On day 113 of gestation, 4 male cloned pigs were obtained from 1 recipient (P177) via cesarean section (Figure 2B). The body weight and length of the 4 piglets ranged from 0.56 to 1.16 kg and 22 to 28 cm, respectively. The other recipient (P178) miscarried at 46 d of gestation.

PCR genotyping and DNA sequence analyses of the 4 cloned pigs showed that all 4 pigs had the same mutation as the nuclear donor cells (3-bp substitution and 86-bp deletion; Figure 2C and D). Western blot analyses further showed that all 4 pigs lacked the IL2RG protein (Figure 2E).

Phenotypic characterization of *IL2RG* KO pigs

Gross anatomical analysis revealed that all 4 *IL2RG* KO pigs completely lacked thymuses (Figure 3A, B). Histological analysis of the spleens clearly showed the presence of lymphocytes in the white pulp of the peripheral lymphoid sheath tissue (PALS) in wild-type (WT) pigs (Figure 3C), whereas the *IL2RG* KO pigs showed very few or no lymphocytes in the PALS (Figure 3D). Embryonic hematopoiesis in the red pulp was strong in both WT and *IL2RG* KO pigs (data not shown). The lymphocyte counts in the peripheral blood of the WT and *IL2RG* KO pigs were $15.7\pm2.2\times10^2$/ μl and $6.5\pm3.0\times10^2$/ μl, respectively, indicating a significant reduction in the lymphocyte number in *IL2RG* KO pigs ($P<0.01$; Figure 3E).

Flow cytometric analyses of the peripheral blood (Figure 4A) showed that the number of $CD3^+$ T cells in *IL2RG* KO pigs ($0.3\%\pm0.1\%$) was drastically lower than that in WT pigs ($74.0\%\pm10.2\%$; $P<0.0001$). In addition, *IL2RG* KO pigs lacked $CD3^+CD4^+$ and $CD3^+CD8^+$ T cells. The number of NK cells (monocyte/granulocyte$^-$, $CD3^-$, and $CD16^+$) was also notably lower in *IL2RG* KO pigs than WT pigs (*IL2RG* KO, $0.9\%\pm0.2\%$ vs. WT, $8.1\pm4.5\%$; $P=0.004$), although the B cell population ($CD3^-$ and $CD45RA^+$) in *IL2RG* KO pigs was observed to be the same as that in WT pigs. As observed in the peripheral blood, the numbers of splenic T cells (*IL2RG* KO, $0.2\%\pm0.1\%$ vs. WT, $28.1\%\pm10.9\%$; $P<0.0001$) and NK cells (*IL2RG* KO, $0.8\%\pm0.3\%$ vs. WT, $3.9\%\pm0.8\%$; $P=0.0001$) were significantly reduced in *IL2RG* KO pigs (Figure 4B). Thus, an almost complete lack of T and NK cells was observed in the *IL2RG* KO pigs, which is similar to human XSCID patients.

Discussion

In rodents, the microinjection of ZFN-encoding mRNA into fertilized eggs has been used for the creation of gene KO animals, mainly due to its simplicity. However, the drawbacks of this microinjection method include inefficiency and the occurrence of mutation mosaicism [24]. The transfer of mRNA-injected eggs into recipient females gives rise to both non-mutant and mutant offspring, and the generation of mutants results in undesired mutations that are meaningless with regard to the traits of the gene KO animals. Mutation mosaicism can result from sustained ZFN activity during later embryogenesis or the re-cleavage of the already-modified alleles [33,34]. Individuals with the desired mutation can be selected after crossbreeding with WT animals. Such a breeding process, however, requires enormous time, labor, and costs in large animals such as pigs, which have longer gestation intervals than rodents. We therefore applied the gene KO procedure using SCNT for the generation of *IL2RG* KO pigs in the present study. With this method, nuclear donor cells could be examined *in vitro* for the induced mutations prior to the production of cloned animals by SCNT [2]. Thus, the wasteful production of undesired animals can be avoided. To our knowledge, this study is the first to demonstrate the generation of cloned pigs from gene KO cells prepared using ZFN-encoding mRNA.

For the generation of gene KO pigs by somatic cell cloning, HR has traditionally been used to knock out a target gene in nuclear donor cells [11,12,29]. In HR, an antibiotic-based cell selection is performed to obtain KO cells; however, several issues arise, including (1) the insertion of an antibiotic cassette into the host genome using targeting vectors, (2) the senescence or exhaustion of nuclear donor cells caused by the prolonged culture associated with antibiotic selection, and (3) the unavoidable contamination of non-targeted cells despite the positive–negative screening [29,35–37]. Therefore, a re-cloning process, namely repeated nuclear transfer, is often necessary to obtain KO offspring [38,39]. In the re-cloning process, fetuses are collected after the first round of SCNT and embryo transfer, and these first-round cloned fetuses can be analyzed for gene KO status. The establishment of primary

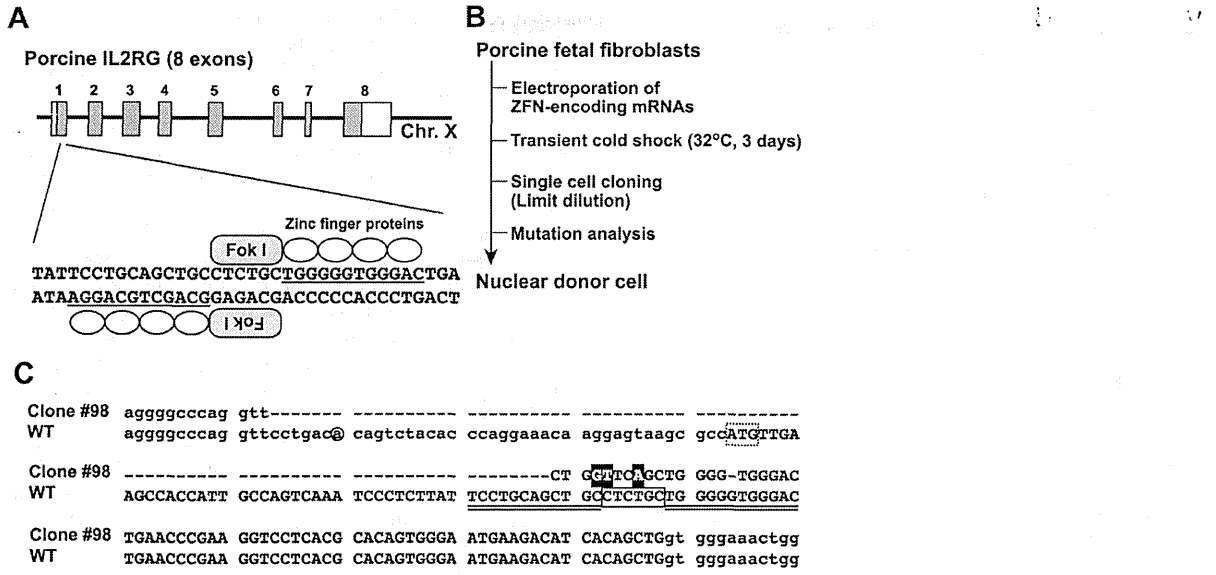

Figure 1. Design of ZFNs targeting the pig *IL2RG* gene and isolation of nuclear donor cells. (A) Schematic representation of ZFNs binding to pig *IL2RG*. The coding and untranslated regions are indicated by gray and white boxes, respectively. A ZFN consists of a nuclease domain (Fok I) and a DNA-binding domain (zinc finger proteins), and the recognition sequences of the zinc finger proteins are underlined. (B) Flow chart for the isolation of nuclear donor cells (clone #98) for SCNT. (C) ZFN-induced mutation in cell clone #98. The upper and lower sequences represent the WT and clone #98 sequence of *IL2RG*, respectively. The deletion mutation and nucleotide substitution in clone #98 are indicated by a hyphen and black box, respectively. The initiation codon of *IL2RG* is shown in a dotted box. The ZFN-binding and ZFN-cleavage sites are double-underlined and boxed, respectively. The major transcription initiation site is indicated with a circle.
doi:10.1371/journal.pone.0076478.g001

culture cells from the gene KO fetus requires obtaining rejuvenated nuclear donor cells for the next round of SCNT. Using these rejuvenated cells, the antibiotic cassette can be excised, provided that the proper site-specific recombinase technology, such as Cre-*lox*P recombination, was incorporated [40].

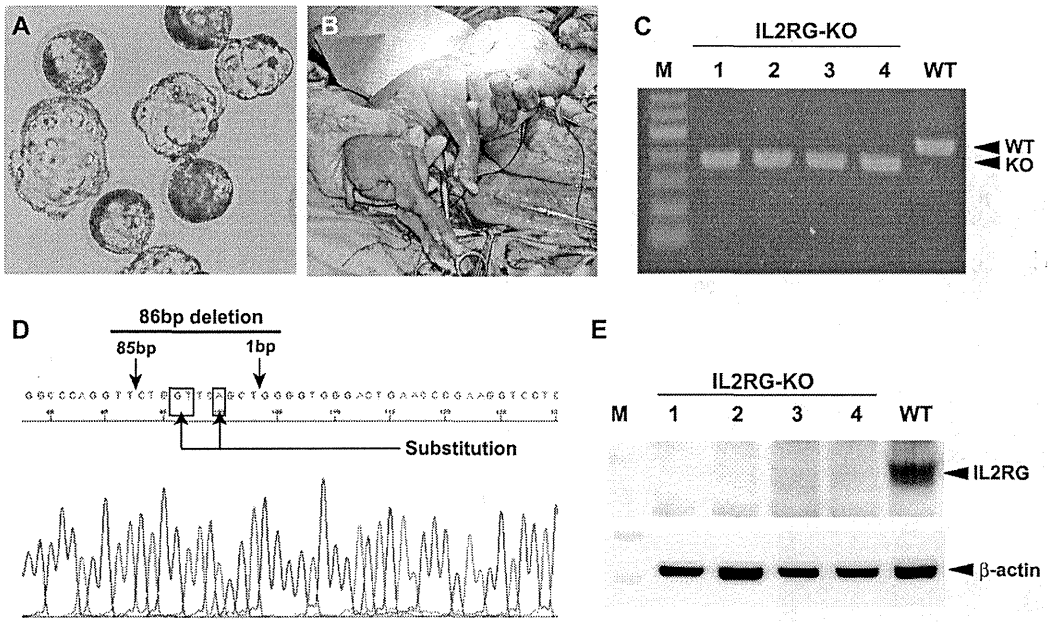

Figure 2. Generation and analysis of *IL2RG* KO pigs. (A) Cloned blastocysts transferred to recipient gilts. (B) Cloned *IL2RG* KO pig delivered by cesarean section at 113 d of gestation. (C) PCR genotyping for the 4 cloned piglets obtained. M: DNA marker. (D) The DNA sequence analysis of *IL2RG* in a cloned pig. The arrows and boxes indicate the same mutation as that of the nuclear donor cell (clone #98). (E) Western blot for IL2RG protein in the spleens of *IL2RG* KO pigs. β-actin was used as a loading control. M: protein standard marker.
doi:10.1371/journal.pone.0076478.g002

Table 1. *in vitro* development of SCNT embryos and production of *IL2RG* KO pigs.

in vitro development of reconstructed SCNT embryos		
SCNT embryos reconstructed	403	
Normally cleaved embryos on day 2	151 (71.9%)	
Blastocyst-stage embryos on day 5	237 (58.8%)	
Production of *IL2RG* KO pigs		
Recipient	P177	P178
Blastocysts transferred[a]	100	99
Pregnancy	+	+
Cloned fetuses obtained	4 (4.0%)	- (miscarried)[b]

[a]Day 5–6 embryos.
[b]46 d of gestation.
doi:10.1371/journal.pone.0076478.t001

In contrast, ZFN-encoding mRNAs can generate gene KO cells without antibiotic selection. In fact, sufficient numbers of nuclear donor cells for SCNT can be obtained in a short period of time (approximately 3 weeks). Moreover, the *IL2RG*-KO cells generated by the ZFN-encoding mRNAs in this study allowed for the direct production of full-term cloned fetuses without rejuvenation of the nuclear donor cells and subsequent re-cloning. As a result, we obtained full-term cloned fetuses within 6 months, including the period spent establishing the KO cells, whereas the HR method requires an average of 12 to 18 months to obtain KO animals. An additional advantage of ZFN-encoding mRNAs is transient ZFN expression, which reduces the incidence of off-target mutations [41]. Off-target events are a potential limitation of the ZFN technique [26,42,43], although the introduction of ZFN-encoding mRNAs leads to the immediate translation of ZFNs in the cytoplasm without the risk of genomic integration, which could disrupt endogenous genes. Carlson et al. recently generated KO pigs using TALEN-encoding mRNA [44]. Based on these collective results, we believe that it is important to compare the efficiencies of ZFN- and TALEN-mRNA in generating KO pigs.

A marked decrease in the number of T and B cells has been reported in XSCID mice [45,46] and rats [24]. In human XSCID patients, although the number of T and NK cells is significantly decreased, the number of B cells remains normal or is occasionally increased [28,47]. Thus, the phenotypes of rodent XSCID models do not necessarily mimic the conditions of human XSCID. In contrast, the *IL2RG* KO pigs obtained in this study lacked T and NK cells but showed normal B cell populations, and identical phenotypic characteristics were shown in a previous report in which XSCID pigs were generated through HR [29]. Thus, *IL2RG* KO pigs are considered to be an accurate model that mimics human XSCID.

Opportunistic infections in XSCID animals after birth are unavoidable under conventional housing conditions. We therefore used the full-term *IL2RG* KO pig fetuses recovered via cesarean section (113 d of gestation) for our analyses to avoid any changes due to infections.

In conclusion, this study presents a simple, non-integrating strategy for generating KO pigs using ZFN-encoding mRNA, which successfully generated *IL2RG* KO pigs via the SCNT method in a short period of time. The combination of ZFN-encoding mRNA with SCNT provides a robust method for generating KO pigs without genomic integration. Moreover, the resulting *IL2RG* KO pigs showed a phenotype similar to that of human XSCID. Although further characterization is required, these findings represent the first step toward developing a porcine SCID model, and we believe that this *IL2RG* KO pig model will greatly contribute not only to cancer and stem cell research but also to preclinical evaluations of the transplantation of pluripotent stem cells, such as iPS cells.

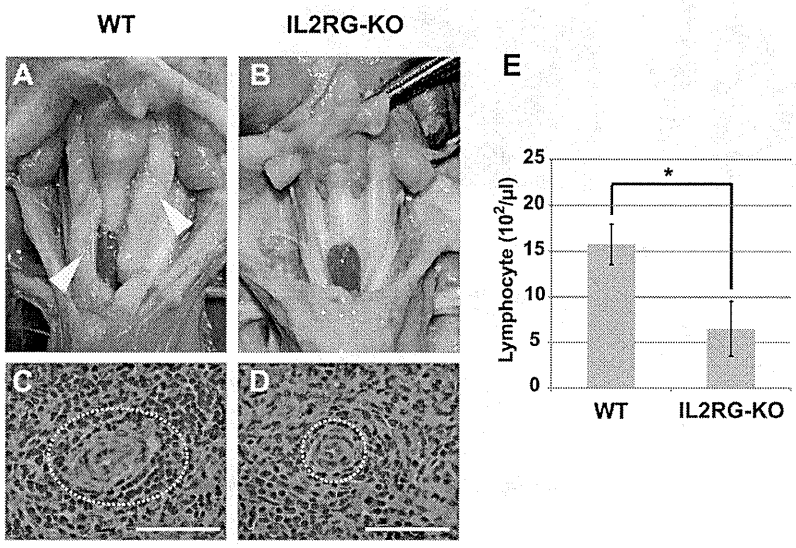

Figure 3. Phenotypes of *IL2RG* KO pigs. (A, B) The thymic phenotype in WT and *IL2RG* KO pigs. The white arrowheads indicate normal thymuses in WT pigs. (C, D) Histological analysis of the spleens of WT and *IL2RG* KO pigs. The white pulp of the spleen is indicated by a dotted white circle. Bar = 100 μm. (E) The proportion of lymphocytes in the peripheral blood (PB) of WT and *IL2RG* KO pigs. The data represent the means ± SD values for 4 pigs. The asterisk indicates a statistically significant difference ($P<0.01$) between the values for WT and *IL2RG* KO pigs (n = 4).
doi:10.1371/journal.pone.0076478.g003

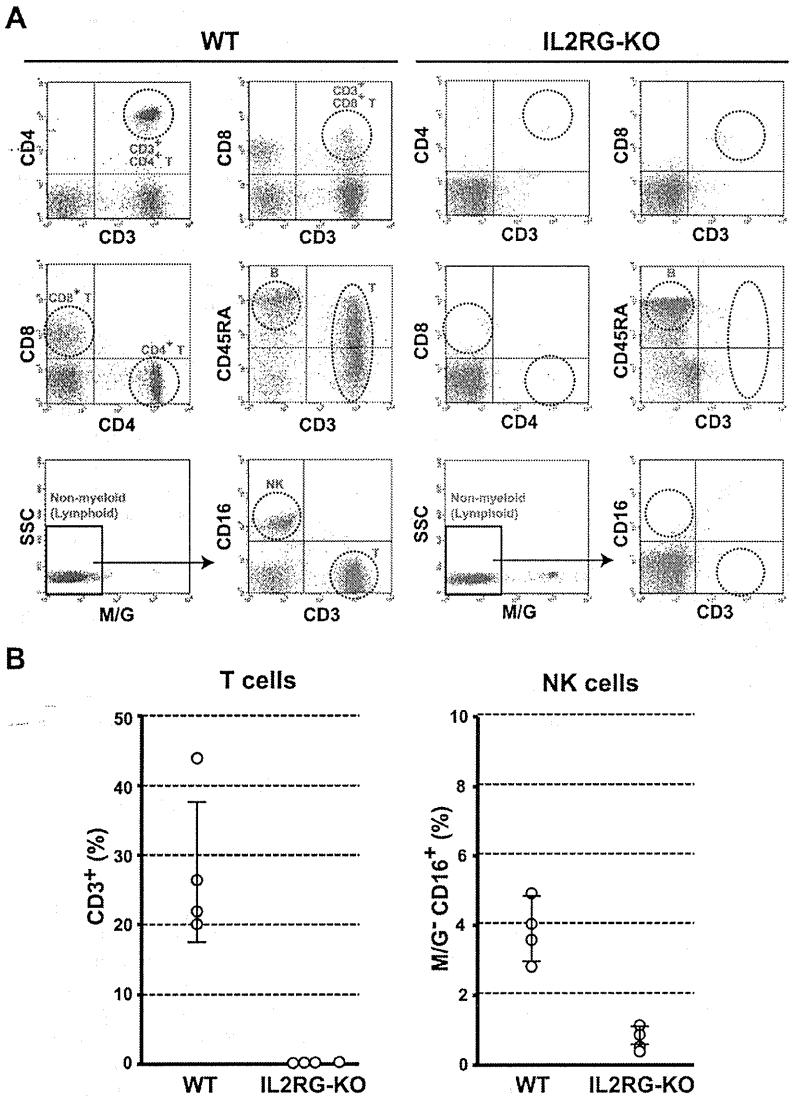

Figure 4. Flow cytometric analysis of mononuclear cells in *IL2RG* KO pigs. (A) Flow cytometric analysis of T, B, and NK cells in the peripheral blood of *IL2RG* KO pigs. The dot plots show CD3, CD4, and CD8 cells for the demarcation of T cell subpopulations and CD3, CD45RA, and CD16 (in the non-myeloid fraction, i.e., monocyte/granulocyte (M/G)-negative) cells for the differentiation of T cell, B cell, and NK cell subpopulations in the peripheral blood, respectively. (B) The proportion of T ($CD3^+$) and NK (M/G^-, $CD3^-$, $CD16^+$) cells among the mononuclear cells in the spleens of *IL2RG* KO pigs. The data represent the mean ± SD values of the 4 pigs obtained.
doi:10.1371/journal.pone.0076478.g004

Materials and Methods

Animal care and chemicals

All of the animal experiments in this study were approved by the Institutional Animal Care and Use Committee of Meiji University (IACUC10-0004). All chemicals were purchased from the Sigma-Aldrich Chemical Co. (MO, USA) unless otherwise indicated.

Design of ZFNs and mRNA preparation

Custom ZFN plasmids for pig *IL2RG* were obtained from Toolgen Inc. The design and validation of these ZFNs was performed by Toolgen Inc (Seoul, South Korea). The constructed ZFNs were designed to target the sequence of exon 1 in the pig *IL2RG* gene. Each of the ZFNs had 4 zinc finger domains recognizing 12 bases (Figure 1). For the production of ZFN-encoding mRNA, each of the ZFN plasmids was digested with the restriction enzyme Xho I. The linearized plasmids were then purified with phenol/chloroform to generate a high-quality DNA template for *in vitro* transcription. Capped ZFN mRNA was produced from the linearized DNA template via *in vitro* transcription using a MessageMAX T7 ARCA-Capped Message Transcription Kit (Cambio, Cambridge, UK). A poly(A) tail was then added to each mRNA by polyadenylation using the Poly(A) Polymerase Tailing Kit (Cambio). The poly(A)-tailed ZFN-encoding mRNA was then purified using a spin column with the MEGAclear Kit (Life Technologies, CA, USA) and finally resuspended in RNase-free water at 400 ng/ μl.

Isolation of *IL2RG* KO cells and culture conditions

A primary culture of porcine fetal fibroblast cells (male line) was used as the progenitor line for the isolation of *IL2RG* KO cells. The fibroblast cells and their derivatives (KO cells) were seeded onto type I collagen-coated dishes or plates (Asahi Glass, Tokyo, Japan) and cultured in MEMα (Life Technologies) supplemented with 15% FBS (Nichirei Bioscience, Tokyo, Japan) and 1× antibiotic-antimycotic solution (Life Technologies) in a humidified atmosphere containing 5% CO_2 at 37°C. The fetal fibroblasts were cultured to 70–90% confluence, washed twice with D-PBS(−) (Life Technologies), and treated with 0.05% trypsin-EDTA (Life Technologies) to isolate and collect the cells. The cells (4×10^5) were then suspended in 40 µl of R buffer (supplied as part of the Neon Transfection System, Life Technologies), and 2 µl of ZFN-encoding mRNA solution (400 ng/ µl) was added. The cells were then electroporated under the following conditions: pulse voltage, 1,100 V; pulse width, 30 ms; and pulse number, 1 (program #6). Following electroporation, the cells were cultured at 32°C for 3 d (transient cold shock) first without antibiotics in the medium described above for 24 h and then with antibiotics in the medium [31]. For recovery after the transient cold shock treatment, the cells were cultured at 37°C until they approached confluence, and then limiting dilution was performed to obtain single cell-derived clones in five 96-well plates. At 12 d after limiting dilution, cells at relatively high confluency (>50%) in each well were selected and divided for further culture and mutation analysis. The cells at low confluency (~50%) after limiting dilution were not used in further experiments.

Analysis of ZFN-induced mutations in nuclear donor cells and cloned fetuses

The target region of IL2RG-ZFNs was amplified by direct PCR from the cell clones using MightyAmp DNA polymerase (Takara Bio, Shiga, Japan) and the corresponding primers (5′-ATAGTGGTGTCAGTGTGATTGAGC and 5′-TACGAACT-GACTTATGACTTACC). Nested PCR was then performed using PrimeSTAR HS DNA polymerase (Takara Bio) and the appropriate primers (5′-ATACCCAGCTTTCGTCTCTGC and 5′-TTCCAGAATTCTATACGACC). Subsequently, the PCR fragment including the ZFN target region was examined using the sequencing primer 5′-AGCCTGTGTCATAGCATAC, the BigDye Terminator Cycle Sequencing Kit, and an ABI PRISM 3100 Genetic Analyzer (Life Technologies). For analysis of the mutation in cloned fetuses, genomic DNA was extracted from the tail biopsies of fetuses using a DNeasy Tissue and Blood Kit (QIAGEN, Hilden, Germany), and then PCR genotyping and DNA sequencing were performed as described above. All new sequence data is deposited in DDBJ/EMBL/GenBank (AB846644-AB846648).

SCNT and embryo transfer

SCNT was performed as described previously with slight modifications [32]. Briefly, *in vitro*-matured oocytes containing the first polar body were enucleated via the gentle aspiration of the polar body and the adjacent cytoplasm using a beveled pipette in 10 mM HEPES-buffered Tyrode lactose medium containing 0.3% (w/v) polyvinylpyrrolidone (PVP), 0.1 µg/ml demecolcine, 5 µg/ml cytochalasin B (CB), and 10% FBS. Fibroblasts (clone #98) were used as nuclear donors following cell cycle synchronization via serum starvation for 2 d. A single donor cell was inserted into the perivitelline space of an enucleated oocyte. The donor cell-oocyte complexes were placed in a solution of 280 mM mannitol (Nacalai Tesque, Kyoto, Japan) (pH 7.2) containing 0.15 mM $MgSO_4$, 0.01% (w/v) PVA, and 0.5 mM HEPES and were held between 2 electrode needles. Membrane fusion was induced with a somatic hybridizer (LF201; NEPA GENE, Chiba, Japan) by applying a single direct-current (DC) pulse (200 V/mm, 20 µs) and a pre- and post-pulse alternating current (AC) field of 5 V at 1 MHz for 5 s. The reconstructed embryos were cultured in NCSU23 medium supplemented with 4 mg/ml BSA for 1 to 1.5 h, followed by electrical activation. The reconstructed embryos were then washed twice in an activation solution containing 280 mM mannitol, 0.05 mM $CaCl_2$, 0.1 mM $MgSO_4$, and 0.01% (w/v) PVA and were aligned between 2 wire electrodes (1.0 mm apart) of a fusion chamber slide filled with the activation solution. A single DC pulse of 150 V/mm was applied for 100 µs using an electrical pulsing machine (Multiporator; Eppendorf, Hamburg, Germany). After activation, the reconstructed embryos were transferred into PZM5 supplemented with 5 µg/ml CB and 500 nM Scriptaid for 3 h. The embryos were then transferred into PZM5 supplemented with Scriptaid and further cultured for 12 to 14 h. After incubation, the embryos were further cultured in PZM5, and the dish was maintained under a humidified atmosphere of 5% CO_2, 5% O_2, and 90% N_2 at 38.5°C. Beyond the morula stage, the embryos were cultured in PZM5 supplemented with 10% FBS.

Crossbred (Large White/Landrace × Duroc) prepubertal gilts weighing 100 to 105 kg were used as recipients of the SCNT embryos. The gilts were given a single intramuscular injection of 1,000 IU of eCG to induce estrus. Ovulation was induced by an intramuscular injection of 1,500 IU of hCG (Kawasaki Pharmaceutical, Kanagawa, Japan) that was given 66 h after the injection of eCG. The SCNT embryos cultured for 5 to 6 d were surgically transferred into the oviducts of the recipients approximately 146 h after hCG injection.

Western blot analysis

After the *IL2RG* KO and age-matched WT pigs were sacrificed, their dissected spleens were homogenized in RIPA buffer (Thermo Scientific, MA, USA) with a protease inhibitor cocktail (Nacalai Tesque) and subjected to centrifugation, and the supernatants were collected. The protein concentrations of the samples were quantified using a DC protein assay (Bio-Rad, CA, USA) based on the Lowry method. Approximately 40 µg of protein from the spleen extracts was subjected to 10% SDS-PAGE and transferred by electroblotting to a Hybond-P PVDF membrane (GE Healthcare Bio-Sciences, NJ, USA). The membranes were blocked for 30 min at room temperature with Blocking One (Nacalai Tesque). After blocking, the membranes were incubated with an anti-IL2RG antibody (1:200 dilution; Santa Cruz Biotechnology, CA, USA) for 1 h at room temperature and were subsequently incubated with HRP-conjugated anti-rabbit IgG antibody (1:5,000 dilution; Santa Cruz Biotechnology) for 1 h at room temperature. The blot was developed using ECL Western Blotting Detection Reagents (GE Healthcare Bio-Sciences). The signal was detected and imaged with an ImageQuant LAS-4000 system (GE Healthcare Bio-Sciences).

Flow cytometric analysis

Peripheral blood mononuclear cells were harvested from the whole blood and spleens of *IL2RG* KO pigs using the erythrocyte lysis solution PharmLyse (Becton Dickinson, BD, NJ, USA), and 1×10^6 cells were incubated with mouse anti-pig CD3e (Abcam, Cambridge, UK), CD4a (BD), CD8a (BD), CD16 (AbDSerotec, NC, USA), CD45RA (AbDSerotec), and monocyte and granulocyte (M/G, Abcam) antibodies for 30 min at room temperature. After incubation, the cell suspension was washed and resuspended

with PBS (−) supplemented with 1% FBS (w/v). The cell populations isolated from the peripheral blood and spleens of *IL2RG*-KO pigs were evaluated using a FACSCalibur flow cytometer (BD) equipped with a 488-nm argon laser. The cell debris and aggregates were gated out of the analysis using bivariate, forward/side scatter (FSC/SSC) parameters. In all analyses, the virtual lymphocyte population was gated, and the gated 1×10^4 events per sample were acquired and analyzed using CELLQuest Pro software (BD).

Histological analysis

After the *IL2RG* KO and age-matched WT pigs were sacrificed, their dissected spleens were fixed in 10% neutral buffered formalin solution (Wako Pure Chemical Industries, Osaka, Japan), embedded in paraffin, sectioned, and stained with hematoxylin and eosin using standard methods.

Acknowledgments

We acknowledge Mr. Hiroshi Kadoi (Kadoi Ltd.) for technical help.

Author Contributions

Conceived and designed the experiments: HN. Performed the experiments: MW KN HM TM MM TK M. Kobayashi YM RS M. Kuramoto GH Y. Asano ST Y. Arai. Analyzed the data: MW KN KU. Wrote the paper: MW MN HN. Final approval of the manuscript: MN YH HN.

References

1. Aigner B, Renner S, Kessler B, Klymiuk N, Kurome M, et al. (2010) Transgenic pigs as models for translational biomedical research. J Mol Med 88: 653–664.
2. Kues WA, Niemann H (2004) The contribution of farm animals to human health. Trends Biotechnol 22: 286–294.
3. Vajta G, Gjerris M (2006) Science and technology of farm animal cloning: state of the art. Anim Reprod Sci 92: 211–230.
4. Lunney JK (2007) Advances in swine biomedical model genomics. Int J Biol Sci 3: 179–184.
5. Matsunari H, Nagashima H (2009) Application of genetically modified and cloned pigs in translational research. J Reprod Dev 55: 225–230.
6. Rogers CS, Stoltz DA, Meyerholz DK, Ostedgaard LS, Rokhlina T, et al. (2008) Disruption of the CFTR gene produces a model of cystic fibrosis in newborn pigs. Science 321: 1837–1841.
7. Umeyama K, Watanabe M, Saito H, Kurome M, Tohi S, et al. (2009) Dominant-negative mutant hepatocyte nuclear factor 1alpha induces diabetes in transgenic-cloned pigs. Transgenic Res 18: 697–706.
8. Renner S, Fehlings C, Herbach N, Hofmann A, von Waldthausen DC, et al. (2010) Glucose intolerance and reduced proliferation of pancreatic beta-cells in transgenic pigs with impaired glucose-dependent insulinotropic polypeptide function. Diabetes 59: 1228–1238.
9. Kragh PM, Nielsen AL, Li J, Du Y, Lin L, et al. (2009) Hemizygous minipigs produced by random gene insertion and handmade cloning express the Alzheimer's disease-causing dominant mutation APPsw. Transgenic Res 18: 545–558.
10. Ross JW, Fernandez de Castro JP, Zhao J, Samuel M, Walters E, et al. (2012) Generation of an inbred miniature pig model of retinitis pigmentosa. Invest Ophthalmol Vis Sci 53: 501–507.
11. Dai Y, Vaught TD, Boone J, Chen SH, Phelps CJ, et al. (2002) Targeted disruption of the alpha1,3-galactosyltransferase gene in cloned pigs. Nat Biotechnol 20: 251–255.
12. Lai L, Kolber-Simonds D, Park KW, Cheong HT, Greenstein JL, et al. (2002) Production of alpha-1,3-galactosyltransferase knockout pigs by nuclear transfer cloning. Science 295: 1089–1092.
13. Elliott RB, Escobar L, Tan PL, Muzina M, Zwain S, et al. (2007) Live encapsulated porcine islets from a type 1 diabetic patient 9.5 yr after xenotransplantation. Xenotransplantation 14: 157–161.
14. Porter AC, Itzhaki JE (1993) Gene targeting in human somatic cells. Complete inactivation of an interferon-inducible gene. Eur J Biochem 218: 273–281.
15. Brown JP, Wei W, Sedivy JM (1997) Bypass of senescence after disruption of p21CIP1/WAF1 gene in normal diploid human fibroblasts. Science 277: 831–834.
16. van Nierop GP, de Vries AA, Holkers M, Vrijsen KR, Goncalves MA (2009) Stimulation of homology-directed gene targeting at an endogenous human locus by a nicking endonuclease. Nucleic Acids Res 37: 5725–5736.
17. Geurts AM, Cost GJ, Freyvert Y, Zeitler B, Miller JC, et al. (2009) Knockout rats via embryo microinjection of zinc-finger nucleases. Science 325: 433.
18. Kim YG, Cha J, Chandrasegaran S (1996) Hybrid restriction enzymes: zinc finger fusions to Fok I cleavage domain. Proc Natl Acad Sci U S A 93: 1156–1160.
19. Watanabe M, Umeyama K, Matsunari H, Takayanagi S, Haruyama E, et al. (2010) Knockout of exogenous EGFP gene in porcine somatic cells using zinc-finger nucleases. Biochem Biophys Res Commun 402: 14–18.
20. Whyte JJ, Zhao J, Wells KD, Samuel MS, Whitworth KM, et al. (2011) Gene targeting with zinc finger nucleases to produce cloned eGFP knockout pigs. Mol Reprod Dev 78: 2.
21. Hauschild J, Petersen B, Santiago Y, Queisser AL, Carnwath JW, et al. (2011) Efficient generation of a biallelic knockout in pigs using zinc-finger nucleases. Proc Natl Acad Sci U S A 108: 12013–12017.
22. Li P, Estrada JL, Burlak C, Tector AJ (2012) Biallelic knockout of the alpha-1,3 galactosyltransferase gene in porcine liver-derived cells using zinc finger nucleases. J Surg Res 181: e39–45.
23. Yang D, Yang H, Li W, Zhao B, Ouyang Z, et al. (2011) Generation of PPARgamma mono-allelic knockout pigs via zinc-finger nucleases and nuclear transfer cloning. Cell Res 21: 979–982.
24. Mashimo T, Takizawa A, Voigt B, Yoshimi K, Hiai H, et al. (2010) Generation of knockout rats with X-linked severe combined immunodeficiency (X-SCID) using zinc-finger nucleases. PLoS One 5: e8870.
25. Carbery ID, Ji D, Harrington A, Brown V, Weinstein EJ, et al. (2010) Targeted genome modification in mice using zinc-finger nucleases. Genetics 186: 451–459.
26. Cui X, Ji D, Fisher DA, Wu Y, Briner DM, et al. (2011) Targeted integration in rat and mouse embryos with zinc-finger nucleases. Nat Biotechnol 29: 64–67.
27. Noguchi M, Yi H, Rosenblatt HM, Filipovich AH, Adelstein S, et al. (1993) Interleukin-2 receptor gamma chain mutation results in X-linked severe combined immunodeficiency in humans. Cell 73: 147–157.
28. Buckley RH (2004) Molecular defects in human severe combined immunodeficiency and approaches to immune reconstitution. Annu Rev Immunol 22: 625–655.
29. Suzuki S, Iwamoto M, Saito Y, Fuchimoto D, Sembon S, et al. (2012) Il2rg Gene-Targeted Severe Combined Immunodeficiency Pigs. Cell Stem Cell 10: 753–758.
30. Honma D, Uenishi H, Hiraiwa H, Watanabe S, Tang W, et al. (2003) Cloning and characterization of porcine common gamma chain gene. J Interferon Cytokine Res 23: 101–111.
31. Doyon Y, Choi VM, Xia DF, Vo TD, Gregory PD, et al. (2010) Transient cold shock enhances zinc-finger nuclease-mediated gene disruption. Nat Methods 7: 459–460.
32. Matsunari H, Watanabe M, Umeyama K, Nakano K, Ikezawa Y, et al. (2012) Cloning of homozygous α1,3-galactosyltransferase gene knock-out pigs by somatic cell nuclear transfer. In: Miyagawa S, editor.Xenotransplantation. Rijeka, Croatia: InTech. pp. 37–54.
33. Tesson L, Usal C, Menoret S, Leung E, Niles BJ, et al. (2011) Knockout rats generated by embryo microinjection of TALENs. Nat Biotechnol 29: 695–696.
34. Sung YH, Baek IJ, Kim DH, Jeon J, Lee J, et al. (2013) Knockout mice created by TALEN-mediated gene targeting. Nat Biotechnol 31: 23–24.
35. Forsberg EJ, Strelchenko NS, Augenstein ML, Betthauser JM, Childs LA, et al. (2002) Production of cloned cattle from in vitro systems. Biol Reprod 67: 327–333.
36. Iguma LT, Lisauskas SF, Melo EO, Franco MM, Pivato I, et al. (2005) Development of bovine embryos reconstructed by nuclear transfer of transfected and non-transfected adult fibroblast cells. Genet Mol Res 4: 55–66.
37. Zakhartchenko V, Mueller S, Alberio R, Schernthaner W, Stojkovic M, et al. (2001) Nuclear transfer in cattle with non-transfected and transfected fetal or cloned transgenic fetal and postnatal fibroblasts. Mol Reprod Dev 60: 362–369.
38. Matsunari H, Onodera M, Tada N, Mochizuki H, Karasawa S, et al. (2008) Transgenic-cloned pigs systemically expressing red fluorescent protein, Kusabira-Orange. Cloning Stem Cells 10: 313–323.
39. Fujimura T, Murakami H, Kurome M, Takahagi Y, Shigehisa T, et al. (2008) Effects of recloning on the efficiency of production of alpha 1,3-galactosyltransferase knockout pigs. J Reprod Dev 54: 58–62.
40. Sternberg N, Hamilton D (1981) Bacteriophage P1 site-specific recombination. I. Recombination between loxP sites. J Mol Biol 150: 467–486.
41. Whyte JJ, Prather RS (2012) Cell Biology Symposium: Zinc finger nucleases to create custom-designed modifications in the swine (Sus scrofa) genome. J Anim Sci 90: 1111–1117.
42. Miller JC, Holmes MC, Wang J, Guschin DY, Lee YL, et al. (2007) An improved zinc-finger nuclease architecture for highly specific genome editing. Nat Biotechnol 25: 778–785.
43. Szczepek M, Brondani V, Buchel J, Serrano L, Segal DJ, et al. (2007) Structure-based redesign of the dimerization interface reduces the toxicity of zinc-finger nucleases. Nat Biotechnol 25: 786–793.
44. Carlson DF, Tan W, Lillico SG, Stverakova D, Proudfoot C, et al. (2012) Efficient TALEN-mediated gene knockoutnin livestock. Proc Natl Acad Sci U S A 109: 17382–17387.

45. Cao X, Shores EW, Hu-Li J, Anver MR, Kelsall BL, et al. (1995) Defective lymphoid development in mice lacking expression of the common cytokine receptor gamma chain. Immunity 2: 223–238.
46. DiSanto JP, Muller W, Guy-Grand D, Fischer A, Rajewsky K (1995) Lymphoid development in mice with a targeted deletion of the interleukin 2 receptor gamma chain. Proc Natl Acad Sci U S A 92: 377–381.
47. Sugamura K, Asao H, Kondo M, Tanaka N, Ishii N, et al. (1996) The interleukin-2 receptor gamma chain: its role in the multiple cytokine receptor complexes and T cell development in XSCID. Annu Rev Immunol 14: 179–205.

Human Molecular Genetics, 2013, Vol. 22, No. 21 *4368–4382*
doi:10.1093/hmg/ddt287
Advance Access published on June 19, 2013

Dystrophin-deficient pigs provide new insights into the hierarchy of physiological derangements of dystrophic muscle

Nikolai Klymiuk[1,†], Andreas Blutke[3,†], Alexander Graf[2,†], Sabine Krause[4], Katinka Burkhardt[1], Annegret Wuensch[1], Stefan Krebs[2], Barbara Kessler[1], Valeri Zakhartchenko[1], Mayuko Kurome[1], Elisabeth Kemter[1], Hiroshi Nagashima[5], Benedikt Schoser[4], Nadja Herbach[3], Helmut Blum[2], Rüdiger Wanke[3], Annemieke Aartsma-Rus[6], Christian Thirion[4], Hanns Lochmüller[7,‡], Maggie C. Walter[4,‡] and Eckhard Wolf[1,2,‡,*]

[1]Chair for Molecular Animal Breeding and Biotechnology, [2]Laboratory for Functional Genome Analysis (LAFUGA), Gene Centre, [3]Institute of Veterinary Pathology, Centre for Clinical Veterinary Medicine and [4]Friedrich-Baur-Institute, Department of Neurology, LMU Munich, Germany, [5]Laboratory of Developmental Engineering, Meiji University, Kawasaki, Japan, [6]DMD Genetic Therapy Group, Department of Human Genetics, Leiden University Medical Centre, The Netherlands and [7]Institute of Genetic Medicine, Newcastle University, Newcastle upon Tyne, UK

Received March 21, 2013; Revised and Accepted June 14, 2013

Duchenne muscular dystrophy (DMD) is caused by mutations in the X-linked dystrophin (*DMD*) gene. The absence of dystrophin protein leads to progressive muscle weakness and wasting, disability and death. To establish a tailored large animal model of DMD, we deleted *DMD* exon 52 in male pig cells by gene targeting and generated offspring by nuclear transfer. DMD pigs exhibit absence of dystrophin in skeletal muscles, increased serum creatine kinase levels, progressive dystrophic changes of skeletal muscles, impaired mobility, muscle weakness and a maximum life span of 3 months due to respiratory impairment. Unlike human DMD patients, some DMD pigs die shortly after birth. To address the accelerated development of muscular dystrophy in DMD pigs when compared with human patients, we performed a genome-wide transcriptome study of biceps femoris muscle specimens from 2-day-old and 3-month-old DMD and age-matched wild-type pigs. The transcriptome changes in 3-month-old DMD pigs were in good concordance with gene expression profiles in human DMD, reflecting the processes of degeneration, regeneration, inflammation, fibrosis and impaired metabolic activity. In contrast, the transcriptome profile of 2-day-old DMD pigs showed similarities with transcriptome changes induced by acute exercise muscle injury. Our studies provide new insights into early changes associated with dystrophin deficiency in a clinically severe animal model of DMD.

INTRODUCTION

Duchenne muscular dystrophy (DMD) is a severe X-linked disease that affects 1 in 3500 males. DMD is caused by loss-of-function mutations in the *DMD* gene (~2.5 Mb, 79 exons) that lead to a shift in its reading frame, out-of-frame transcripts and loss of the essential muscle cytoskeletal protein dystrophin (1). The hotspots for mutations are in the regions of exons 3–7 and of exons 45–55 (2). DMD is characterized by progressive muscle weakness and wasting: patients present first symptoms before the age of 5 years, lose ambulation around the age of 12 years and die of respiratory or heart failure in the second to fourth decade of life (3).

*To whom correspondence should be addressed at: Chair for Molecular Animal Breeding and Biotechnology, Gene Centre, LMU Munich, Feodor-Lynen-Str. 25, D-81377 Munich, Germany. Tel: +49 89218076800; Fax: +49 89218076849; Email: ewolf@lmu.de
†Equally contributing authors.
‡Equally contributing last authors.

While curative treatments are currently not available, genetic and pharmacological approaches are under investigation, some having advanced to early phase clinical trials (4–7).

Existing mouse (8–10) and dog (11) models have been instrumental to understand the pathophysiology of DMD and to develop therapeutic strategies, but have limitations with respect to resemblance of the clinical phenotype and/or the type of mutation (reviewed in 12).

The pig is an established model organism for biomedical research closely resembling the human size, anatomy and physiology (reviewed in 13). Importantly, gene targeting allows the generation of tailored large animal models, as exemplified by the cystic fibrosis pig (14). Here, we report the generation and the clinical, pathological and biochemical characterization of pigs with a targeted deletion of *DMD* exon 52, a frequent mutation in human DMD (15). Transcriptome profiling of skeletal muscle from 2-day-old and 3-month-old DMD pigs provided new insights into the hierarchy of physiological derangements of dystrophic muscle.

RESULTS

Generation of *DMD* exon 52 deficient pigs

A bacterial artificial chromosome (BAC; CH242-9G11) carrying the relevant part of the porcine *DMD* gene was modified by recombineering (16) to replace the region corresponding to human *DMD* exon 52 by a neomycin resistance cassette (Fig. 1A), which is expected to result in a frame shift in the transcript (15). Modified BACs were transfected into primary kidney cells from a 3-month-old male piglet, and cell clones occurring after positive selection were screened by quantitative polymerase chain reaction (PCR) for replacement of *DMD* exon 52. Eight of 381 cell clones (2.1%) were successfully targeted, and 2 of them were used for nuclear transfer. For each cell clone, a pregnancy was established by transfer of cloned embryos into recipient gilts. Four piglets of the first litter were life born, euthanized within 48 h and tissue samples were processed for histological characterization. Genotyping confirmed the absence of *DMD* exon 52 (Fig. 1B). Two piglets of the second litter died during birth due to an obstetric complication, while the other two piglets (#1263, #1264; Fig. 1C) were delivered by caesarean section and survived. *DMD* exon 52 was deleted in these two piglets (Fig. 1B).

DMD exon 52 deficient pigs lack dystrophin and show reduced levels of dystrophin-associated proteins

The *DMD* transcript profile in skeletal muscle was analysed by RNA-sequencing (RNA-Seq). In the DMD samples, exon 52 sequences were entirely missing, but junctions from exons 51 to 53 were detected, leading to a +1 frame shift and two stop codons in exon 53 and four stop codons in exon 54 (Supplementary Material, Fig. S1).

Two monoclonal antibodies against different human dystrophin epitopes showed normal dystrophin staining of muscle fibres of a neonatal WT piglet, whereas in DMD piglets dystrophin staining was negative (Fig. 1D), reflecting the situation in the majority of human DMD patients (17) (Supplementary Material, Fig. S2). A monoclonal spectrin-specific antibody showed membrane integrity of muscle fibres in WT and DMD piglets (Fig. 1D). Immunoblot analysis confirmed the absence of dystrophin in skeletal muscle of DMD piglets (Fig. 1E).

Since dystrophin-associated proteins (DAPs) are reduced in DMD patients (reviewed in 18), we evaluated the abundance of α-sarcoglycan and β-dystroglycan in skeletal muscle of DMD piglets by immunofluorescence analysis. The levels of both DAPs were clearly reduced in DMD pigs as in DMD patients (Supplementary Material, Fig. S2).

Dystrophin-deficient pigs exhibit striking muscle weakness

DMD piglets #1263 and #1264 showed reduced mobility when compared with age-matched WT controls, but were able to move and feed on their own. At the age of 3 days, their serum creatine kinase (CK) levels were largely elevated (1649 and 2117 versus 210 ± 112 U/l in 5 age-matched WT controls). #1264 died from an intestinal infection at the age of 2 weeks.

Locomotion studies of DMD pig #1263 were performed at the age of 9 weeks using a size-matched WT pig as a control. The mobility of the DMD pig was disturbed in all three gaits (walk, trot, gallop), with shortened strides and stiff movements being the most prominent features (Supplementary Material, Video S1). While the WT pig easily mastered repeatedly jumping up and down a platform (height 25 cm), the DMD pig failed to climb the platform (Fig. 1F and Supplementary Material, Video S1), demonstrating striking muscle weakness.

Severity of the DMD phenotype correlates with birth weight

To address the clinical phenotype of DMD pigs systematically, we performed a second series of nuclear transfer experiments, resulting in a total of 22 DMD piglets ($n = 9$, 9 and 4 per litter). The cloned piglets showed a large variation in birth weight, which is a finding known to be associated with nuclear transfer technology (19) and is not related to the *DMD* mutation. Interestingly, we observed a negative correlation between birth weight and life expectancy (Fig. 2A). Animals with a birth weight of more than 1200 g died within the first few days. DMD piglets with the highest birth weight (1820–1980 g) were most severely affected and could not move at all (Fig. 2A and Supplementary Material, Video S2). The clinical symptoms suggested muscle weakness and breathing problems as primary causes of death. In contrast, the life expectancy of five animals with a relatively low birth weight was in the range of 3 months, as observed for DMD piglet #1263 from the first SCNT series. At the age of 4 weeks, their serum CK values ranged between 21 000 and 63 000 U/l. Additional locomotion studies performed in two 10-week-old DMD pigs confirmed the difficulties in running and climbing (Supplementary Material, Video S3).

DMD pigs exhibit fulminant progressive muscular dystrophy

DMD pigs of different ages and age-matched WT pigs were subjected to systematic pathological analysis. Grossly, DMD pigs displayed pale skeletal muscles of moist texture, with multifocal areas of pale discolouration, especially in the diaphragm and intercostal musculature. Histological examination revealed a

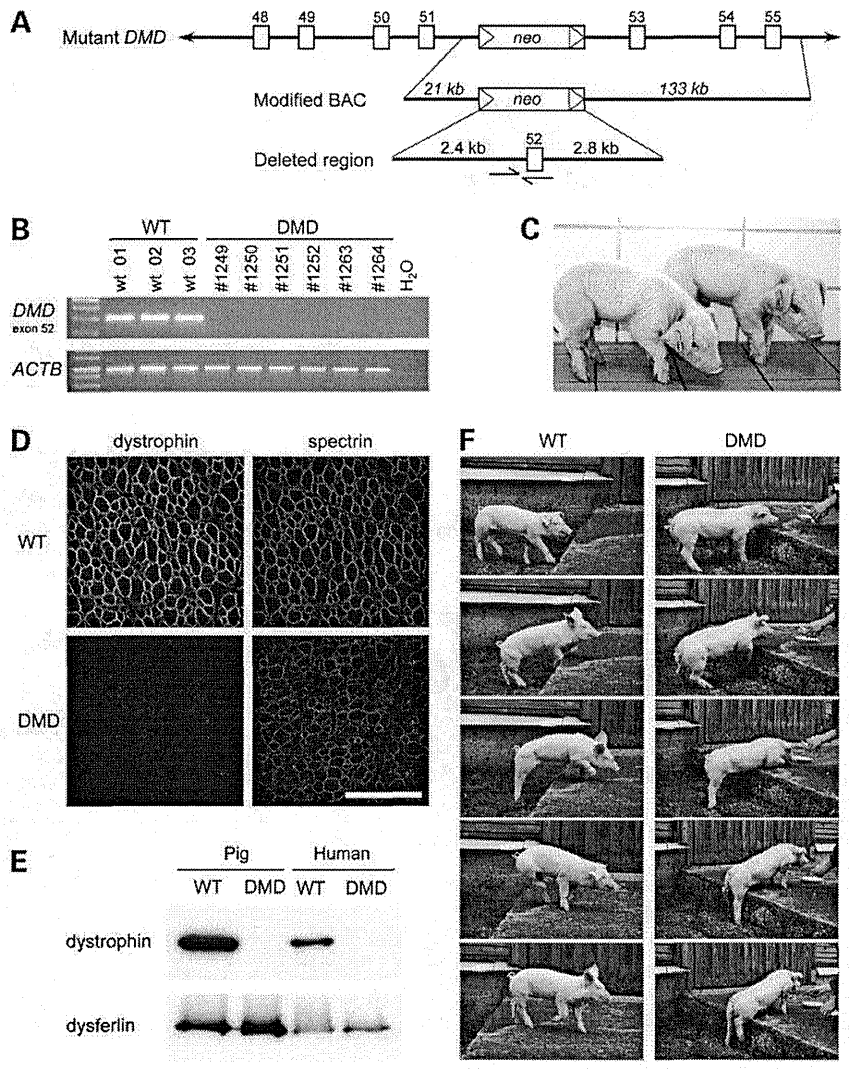

Figure 1. Targeted deletion of exon 52 of the porcine *DMD* gene and consequences for dystrophin expression and muscle function. (**A**) Schematic picture of replacement of exon 52 by a *neo*® cassette to generate the targeting BAC. The primers used to detect the loss of exon 52 are indicated as arrows. (**B**) Genomic PCR analysis demonstrating the loss of *DMD* exon 52 in cloned piglets; WT, wild-type; *ACTB*, β-actin gene. (**C**) Ten-day-old *DMD* mutant pigs. (**D**) Immunofluorescence analysis demonstrating lack of dystrophin expression in biceps femoris muscle of a DMD pig. Anti-spectrin antibodies were used for membrane staining; original magnification ×400; bar = 50 μm. (**E**) Western blot confirming the absence of dystrophin in a DMD pig and a human DMD patient. Anti-dysferlin antibodies were used to control for equal loading within species. (**F**) Inability of a 9-week-old DMD pig to climb a 25 cm platform, demonstrating striking muscle weakness.

myopathy with excessive fibre size variation, numerous large rounded hypertrophic fibres, branching fibres and fibres with central nuclei, as well as scattered clusters of segmentally necrotic fibres, next to hypercontracted fibres and groups of small regenerating muscle fibres. These lesions were accompanied by interstitial fibrosis and mononuclear inflammatory cell infiltration, mimicking the hallmarks of the human disease. The severity and extent of these alterations progressed with age (Fig. 2B) and was most severe in the diaphragm, the laryngeal and intercostal musculature, and triceps brachii muscle. Examination of the heart musculature did not reveal accentuated signs for a cardiac involvement (Fig. 2C).

Morphometric analyses were performed on samples of biceps femoris muscle of 2-day-old and 3-month-old DMD and WT pigs (Fig. 3A). The mean minimal Feret's diameter of muscle fibres was 34% ($P < 0.01$) and 55% ($P < 0.001$) reduced in 2-day-old and 3-month-old DMD pigs when compared with age-matched WT controls (Fig. 3B). Further, the proportion of muscle fibre cross-section profiles with centrally located nuclear section profiles was doubled in 2-day-old DMD pigs and was increased by more than 20-fold in 3-month-old DMD pigs (Fig. 3B). The distribution of muscle fibre diameters from the mean was similar in 2-day-old DMD and WT pigs (Fig. 3C, left panel). In contrast, 3-month-old DMD pigs displayed a broadened, biphasic distribution, with peaks in small and large diameters of fibre size (Fig. 3C, right panel), indicating progressive DMD pathology.

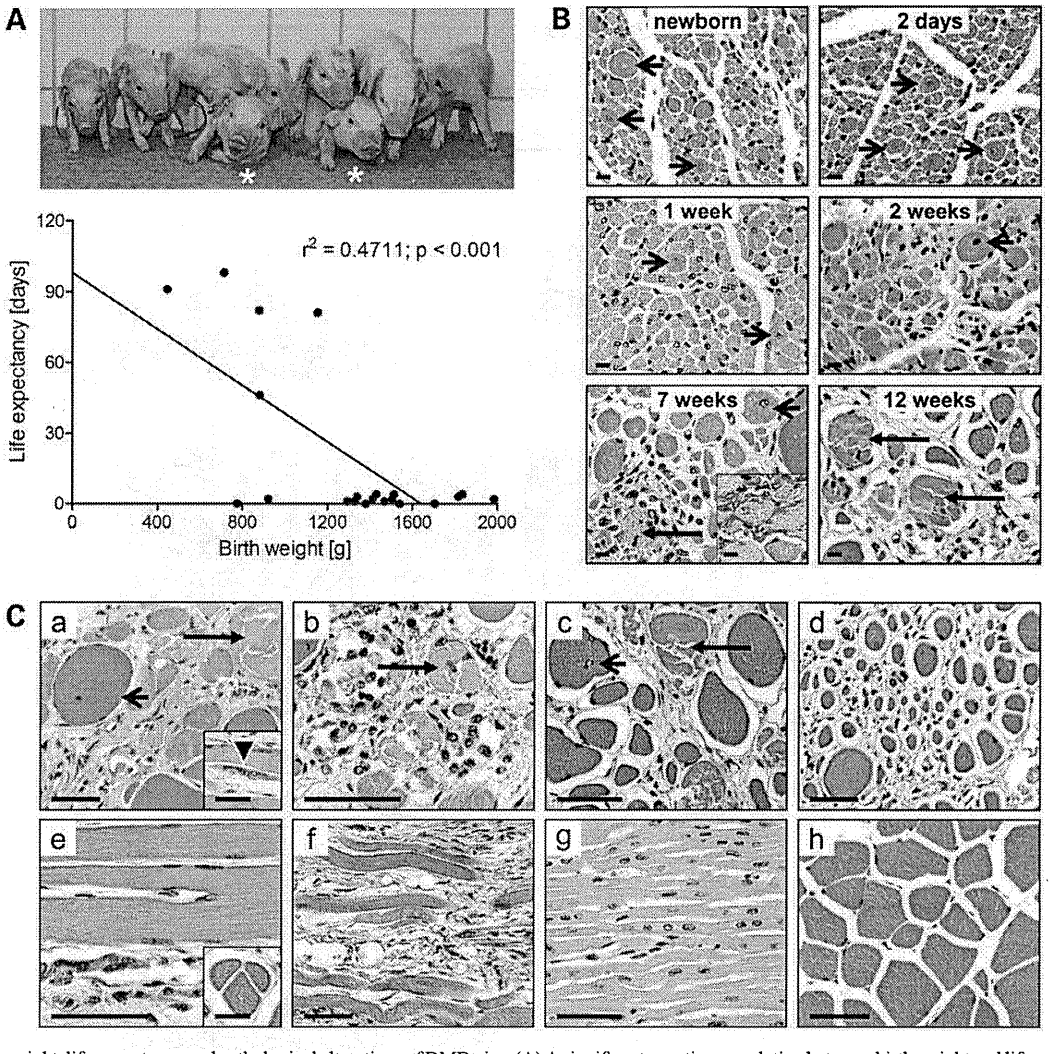

Figure 2. Birth weight, life expectancy and pathological alterations of DMD pigs. (**A**) A significant negative correlation between birth weight and life expectancy was revealed in the 22 DMD pigs of the second series of cloning experiments. Representative pigs are shown in the photograph. Note that pigs with a high birth weight between 1820 and 1980 g (marked by asterisks) were not able to stand or to move (see also Supplementary Material, Video S2). (**B**) Age-related progression of severity of structural alterations in skeletal muscle of DMD pigs of different ages as indicated. Histology of the biceps femoris muscle, paraffin sections, haematoxylin and eosin (H&E)-staining; inset: demonstration of interstitial fibrosis by Masson's trichrome-staining (blue colour). Short arrows indicate large, rounded fibres with internalized central nuclei, long arrows necrosis of muscle fibres. Bars = 10 μm. (**C**) Histopathology of muscles of 3-month-old DMD pigs (a–g) and an age-matched control pig (h). Paraffin sections. H&E-staining (a–e, g, h), Masson's trichrome-staining (f). Bars = 50 μm, bar in inset to e = 10 μm. Cross-sections of the triceps brachii muscle (a, h), the diaphragm (left pillar, b), thyreohyoideus muscle (larynx, c) and longissimus dorsi muscle (d) demonstrating excessive variation of fibre diameters with hypertrophic rounded fibres with centrally located nuclei (short arrows), regeneration of fibres (arrowhead in inset to a) and necrosis of muscle fibres (long arrows) with peri- and endomysial mononuclear (histiocytic) cell infiltration (b). (e) (triceps brachii muscle, longitudinal section; inset: biceps femoris muscle, cross section): Branching/splitting of fibres. (f) (diaphragm, longitudinal section): interstitial fibrosis (blue colour). (g) (heart, left ventricle, longitudinal section): Normal histomorphology.

In summary, the clinical and pathological studies indicate that DMD pigs develop a progressive muscular dystrophy in an accelerated mode when compared with human patients.

Differential expression and localization of utrophin in young versus older DMD pigs

In DMD patients and in the *mdx* mouse model, an up-regulation of dystrophin-related protein (utrophin) has been observed, which can partially compensate the function of dystrophin (reviewed in 20). Thus, we asked if the level of utrophin expression in DMD pigs may contribute to their accelerated phenotype.

Western blot analysis showed a trend of increased utrophin expression in 2-day-old and markedly increased utrophin levels in 3-month-old DMD pigs when compared with age-matched WT pigs (Fig. 4A).

Immunohistochemistry did not detect sarcolemmal utrophin expression in 2-day-old DMD and WT pigs (Fig. 4B). In both groups, blood vessels were strongly stained, probably representing the main source of signal in the western blot analysis. In

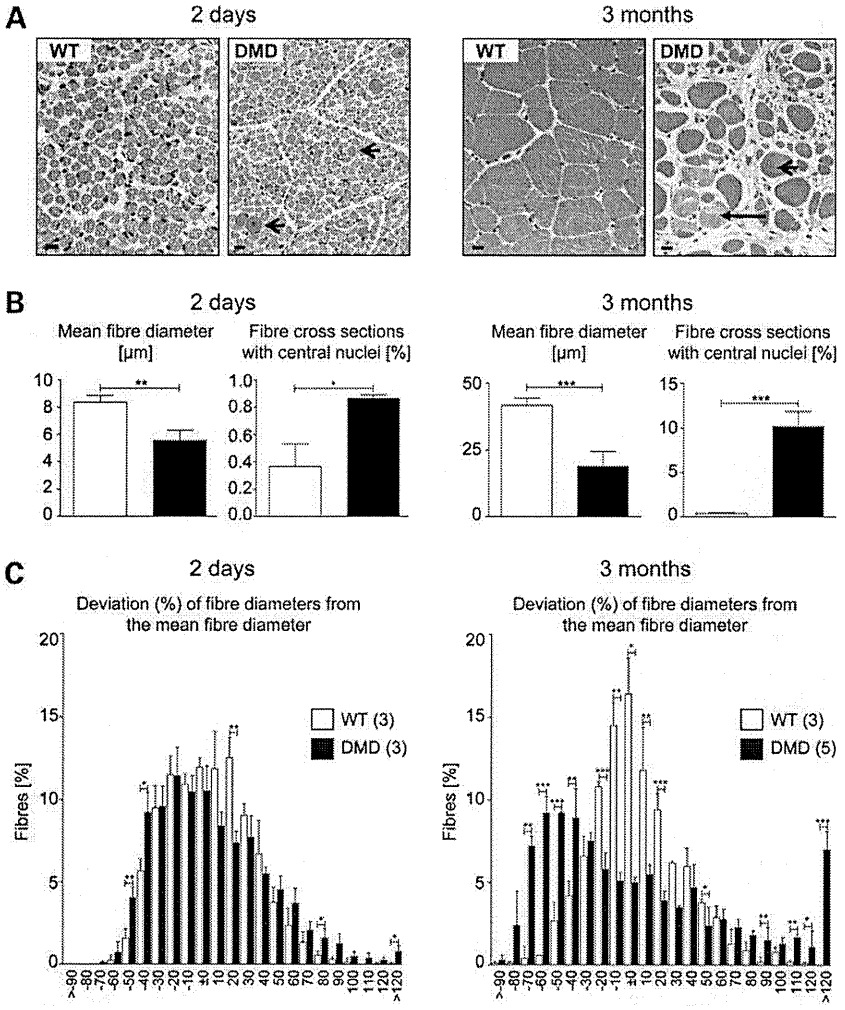

Figure 3. Quantification of structural alterations of skeletal muscle in DMD versus WT pigs at 2 days ($n = 3/3$) and 3 months of age ($n = 5/3$). (**A**) Histology of biceps femoris muscle. Short arrows indicate large, rounded fibres with internalized central nuclei, long arrow necrosis of muscle fibres. Plastic (GMA/MMA) sections, H&E staining; bars = 10 µm. (**B**) Mean minimal Feret's diameter of muscle fibre cross-section profiles (biceps femoris muscle) and proportion of muscle fibre cross-section profiles with central nuclei cross-section profiles. The coefficient of variation in the minimal Feret's diameter was significantly ($P < 0.001$) higher in DMD pigs of both age groups (2 days: 0.38 ± 0.01 versus 0.29 ± 0.02 in WT; 3 months: 0.71 ± 0.05 versus 0.31 ± 0.01 in WT). While the volume density of muscle fibres was not different between 2-day-old DMD and WT piglets, this parameter was significantly ($P < 0.001$) decreased in 3-month-old DMD pigs (0.71 ± 0.04) when compared with age-matched WT pigs (0.96 ± 0.02). (**C**) Distribution of deviations of muscle fibre minimal Feret's diameters from the mean fibre diameter (in classes of 10% deviation) in the biceps femoris muscle. Note the broadened biphasic distribution of muscle fibre diameters in 3-month-old DMD pigs. Data: means ± SD. Significance: $^{*}P < 0.05$; $^{**}P < 0.01$; $^{***}P < 0.001$.

contrast, 3-month-old DMD pigs displayed clear sarcolemmal utrophin staining (Fig. 4B).

Genotype- and age-related transcriptome changes in skeletal muscle

To systematically address the markedly accelerated disease progression in DMD pigs when compared with human DMD patients and *mdx* mouse models, we performed a holistic transcriptome study of biceps femoris muscle from 2-day-old ($n = 4$) and 3-month-old DMD pigs ($n = 3$) and of age-matched WT controls ($n = 3$ per age) using Affymetrix PorGene 1.0 ST arrays. A heat map of the differentially expressed genes (DEGs) among the four groups defined by genotype × age is shown in Figure 5A. The numbers of transcripts with increased and decreased abundance in 2-day-old DMD versus WT pigs were 176 and 67, respectively. The corresponding numbers of DEGs in 3-month-old DMD versus WT pigs were 164 and 35. In addition, a large number of DEGs (77 up- and 148 down-regulated) between 2-day-old and 3-month-old DMD pigs were found (Fig. 5B). These DEGs do not reflect the physiological age-related change of the muscle transcriptome profile, since only 12 (16%) up-regulated and 5 (3%) down-regulated genes were also differentially expressed between 2-day-old and 3-month-old WT pigs (Fig. 5C). Only 11 genes (*LAMA2*, *SMPDL3A*, *PRG4*, *PLSCR4*, *ARID5B*, *ANKRD1*, *ANKRD44*, *TPR*, *CSRP3*, *GABARAPL1*,

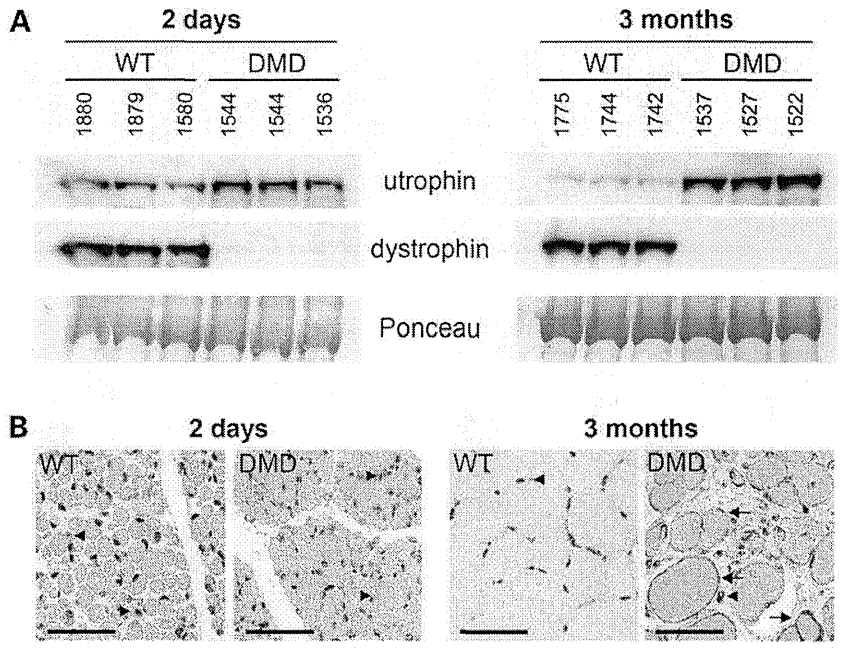

Figure 4. Analysis of utrophin expression in DMD and WT pigs. (**A**) Western blot indicating that utrophin tends to be up-regulated in 2-day-old and is markedly up-regulated in 3-month-old DMD pigs when compared with age-matched WT controls. The Ponceau Red stained membrane is shown to demonstrate equal loading of the lanes. (**B**) Immunohistochemical detection of utrophin in biceps femoris muscle of 2-day-old and 3-month-old DMD pigs and age-matched WT controls. Three-month-old DMD pigs exhibit pronounced sarcolemmal utrophin staining (brown colour, arrows). In 2-day-old DMD and WT pigs, utrophin staining is restricted to blood vessels (arrowheads). Paraffin sections. Bars = 50 μm.

CPM) were commonly overexpressed in both 2-day-old and 3-month-old DMD pigs when compared with age-matched WT pigs, while 5 transcripts (*GADL1*, *MSTN*, *AMPD1*, *EGF*, *DMD*) were reduced in abundance in DMD pigs of both age groups (Fig. 5D), indicating marked differences in the molecular changes associated with the DMD pathology in 2-day-old and 3-month-old animals. Microarray data have been deposited in the GEO database (www.ncbi.nlm.nih.gov/geo/) with the accession number GSE44096.

To get insight into the biological relevance of these transcriptome changes, we performed functional annotation clustering of the DEGs using the Database for Annotation, Visualisation and Integrated Discovery (DAVID) v6.7 (21,22). In addition, we used the tools REVIGO (23) and Cytoscape (24) to visualize enriched gene ontology (GO) terms.

Enriched GO terms for genes overexpressed in 2-day-old DMD versus WT pigs were '(actin) cytoskeleton', 'muscle organ development, actin filament-based movement', 'DNA repair', 'lipid transport' and 'proteolysis' (Fig. 6A; Supplementary Material, Table S1A). GO terms of transcripts with decreased abundance in 2-day-old DMD pigs included 'extracellular matrix', 'extracellular matrix organisation', 'cell adhesion', 'cell cycle/mitosis/cytoskeleton', 'collagen', 'lipid biosynthetic process', 'growth factor', 'vasculature development', 'regulation of cell cycle' and 'regeneration/regulation of growth' (Fig. 6B; Supplementary Material, Table S1B). These transcriptome changes are compatible with the histological findings of muscular dystrophy in the absence of inflammation and fibrosis.

In contrast, highly enriched GO terms of genes overexpressed in biceps femoris muscle of 3-month-old DMD versus WT pigs included 'extracellular region', 'cell adhesion/extracellular matrix', 'lysosome/vacuole', 'proteolysis', 'polysaccharide/heparin binding', 'collagen', 'wound healing', 'cell-matrix adhesion, integrin-mediated signalling pathway', 'cell motion/migration', 'phospholipid binding', 'regulation of apoptosis' and 'adaptive immune response' (Fig. 7A), while 'glucose metabolic process', 'glycolysis' and 'growth factor activity' were enriched GO terms for down-regulated genes in 3-month-old DMD pigs (Fig. 7B). The full list of enriched GO terms of DEGs between 3-month-old DMD and WT pigs is shown in Supplementary Material, Table S2A and B. These molecular changes reflect the progressive muscular dystrophy in 3-month-old DMD pigs, involving degeneration, regeneration, inflammation and reactive fibrosis going along with a severe metabolic disturbance.

This was confirmed by functional annotation clustering of genes differentially expressed between 2-day-old and 3-month-old DMD pigs: enriched GO terms of genes with higher expression in 2-day-old DMD piglets, such as 'cofactor binding', 'mitochondrion', 'aerobic respiration', 'cellular respiration', 'carboxylic acid binding', 'FAD binding' and 'cofactor/coenzyme metabolic process' (Supplementary Material, Table S3A), are compatible with higher metabolic activity, while GO terms of genes with higher transcript levels in 3-month-old DMD pigs (Supplementary Material, Table S3B) reflect the processes of degeneration ('lysosome/vacuole', 'apoptosis'), regeneration ('tube morphogenesis', 'cell motion/migration', 'tube development'), inflammation ('immune response/inflammation', 'adaptive immune response', 'immunoglobulin receptor/binding', 'antigen processing and presentation', 'immunoglobulin') and fibrosis ('extracellular matrix', 'extracellular

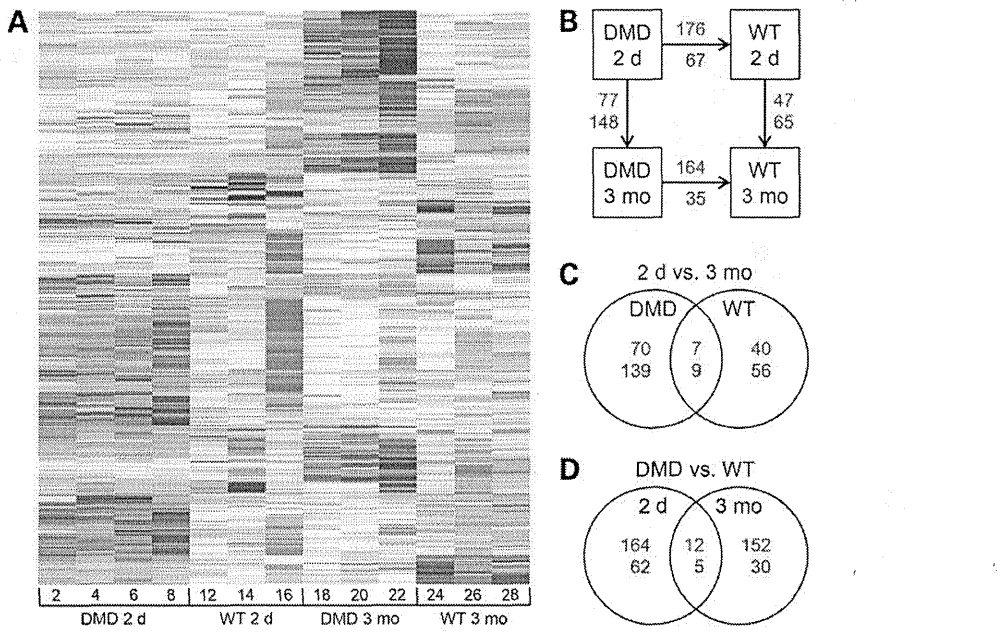

Figure 5. Differential gene expression in biceps femoris muscle of 2-day-old and 3-month-old DMD and WT pigs. (**A**) Heat-map of the DEGs among the four groups defined by genotype × age. Increased abundance of transcripts is indicated in red, decreased abundance in blue colours. (**B**) Number of DEGs between the four groups. Numbers in red and blue indicate the genes up- and down-regulated between the group at the end of an arrow versus the group at the arrow head. (**C**) Age-related transcriptome changes. The numbers in the overlap segment indicate DEGs commonly up- and down-regulated between 2-day-old and 3-month-old pigs of the DMD and WT groups. (**D**) Genotype-related transcriptome changes. The numbers in the overlap segment indicate DEGs commonly up- and down-regulated between DMD and WT pigs of both age classes.

structure organisation', 'collagen'). In WT pigs, the genes expressed at higher levels in 2-day-old animals were summarized by GO term 'extracellular matrix', while in 3-month-old animals transcripts belonging to GO terms 'muscle contraction', 'glucose metabolic process' and 'chloride ion binding' were more abundant (Supplementary Material, Table S4A and B).

Transcriptome changes in skeletal muscle of 3-month-old DMD pigs reflect human DMD and *mdx* mouse muscle

Next, we asked if the transcriptome changes observed in DMD pigs reflect the findings of gene expression studies in skeletal muscle of DMD patients and of the *mdx* mouse. Pescatori *et al.* (25) determined gene expression profiles in muscle biopsies of 19 DMD patients younger than 2 years, thus addressing the pre-symptomatic phase of the disease. Haslett *et al.* (26) investigated the transcriptome of skeletal muscle tissue in DMD children older than 5 years, when impaired muscle function and ambulation becomes clinically manifest. A systematic study of transcriptome changes in skeletal muscle of *mdx* mice between 7 and 112 days of age was performed by Porter *et al.* (27). To compare the changes in gene expression profiles of muscle samples from 2-day-old and 3-month-old DMD pigs versus age-matched controls with these published data sets, we performed gene set enrichment analyses (GSEAs) (28) providing a measure (normalized enrichment score, NES) of the concordance of DEG sets.

The transcripts with increased abundance in 3-month-old DMD pigs were in good concordance with the genes found to be up-regulated in DMD children younger than 2 years (25) (Fig. 7C), older than 5 years (26), and in *mdx* mouse muscles at 23 and 28 days of age (27) (Supplementary Material, Fig. S3A), as indicated by NES >2 with q-values of less than 0.001. A similarly good concordance was found for the down-regulated genes (Supplementary Material, Fig. S3B).

Transcriptomics of 2-day-old DMD pig muscle identifies a mechanical stress signature

The gene expression profiles of biceps femoris muscle samples from 2-day-old DMD piglets were rather different from the published sets of DEGs in DMD patients and in *mdx* mouse muscles (Supplementary Material, Fig. S3C). Specifically, samples from 2-day-old DMD pigs did not display the characteristic transcriptome signatures of ECM remodelling, inflammatory response and decreased energy metabolism which were observed even in DMD patients younger than 2 years, i.e. in the pre-symptomatic period. Instead, the set of transcripts with increased abundance in 2-day-old DMD piglets was similar to a set of genes up-regulated in muscle after acute exercise injury in humans (29) (Fig. 6C) and to transcripts induced by contractile overload (high-force eccentric contractions) in murine skeletal muscle (30) (NES = 1.7624; $q = 0.002$; data not shown).

DISCUSSION

In this study, we generated the first pig model for a genetic muscle disease by gene targeting. In mouse (31) and human

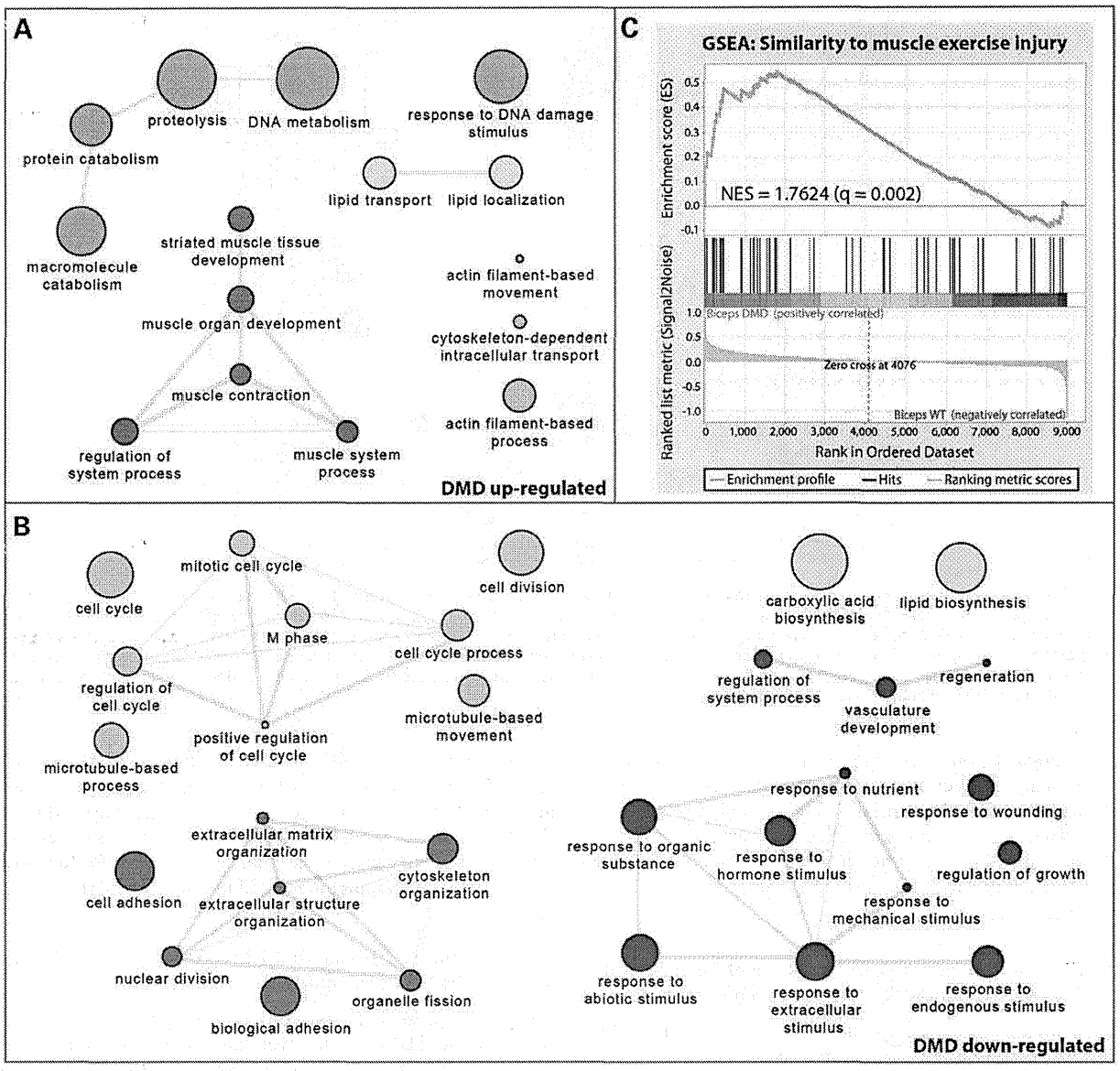

Figure 6. Graph-based visualization of enriched GO terms of genes differentially expressed between DMD and WT pigs at the age of 2 days. (**A**) GO terms of up-regulated and (**B**) GO terms of down-regulated genes in DMD versus WT pigs. The graphs were produced from all significantly enriched GO terms found by DAVID functional annotation clustering using the tools REVIGO (23) and Cytoscape (24). Each GO term is a node in the graph, and 3% of the strongest GO term pairwise similarities are designated as edges in the graph. The generality of GO terms is indicated by bubble size, with smaller bubbles implying more specific terms. (**C**) Gene set enrichment analysis of DEGs up-regulated in 2-day-old DMD pigs versus age-matched WT pigs in a set of genes up-regulated in human skeletal muscle exposed to acute endurance exercise (29). The enrichment profile (green curve) shows a non-random distribution indicated by a roughly triangular outline and a peak close to one of the extremes of the signal-to-noise ordered data set. This distribution means that a higher proportion than expected under the null hypothesis of the genes up-regulated in human skeletal muscle after acute endurance exercise is up-regulated in DMD pigs and fewer than expected are down-regulated or neutral. The leading edge subset containing the most up-regulated genes are the genes positioned left of the peak in the enrichment curve profile. The NES was calculated as outlined in the Materials and Methods section. The *q*-value is the false discovery rate (FDR) corrected *P*-value.

embryonic stem cells (32), a high rate of homologous recombination was observed with large targeting vectors based on BACs, avoiding the need for isogenetic DNA and negative selection markers (reviewed in 33). Therefore, we used a BAC containing the porcine *DMD* exon 52 and replaced it by recombineering (16). After nucleofection of the modified BAC into pre-tested nuclear donor cells, exon 52 replacement was observed in around 2% of the stable nucleofected cell clones, rendering BAC targeting an attractive method for introducing targeted mutations into large animal genomes. Importantly, the two targeted cell clones used for nuclear transfer produced pregnancies and offspring at a rate within the usual range of nuclear transfer in

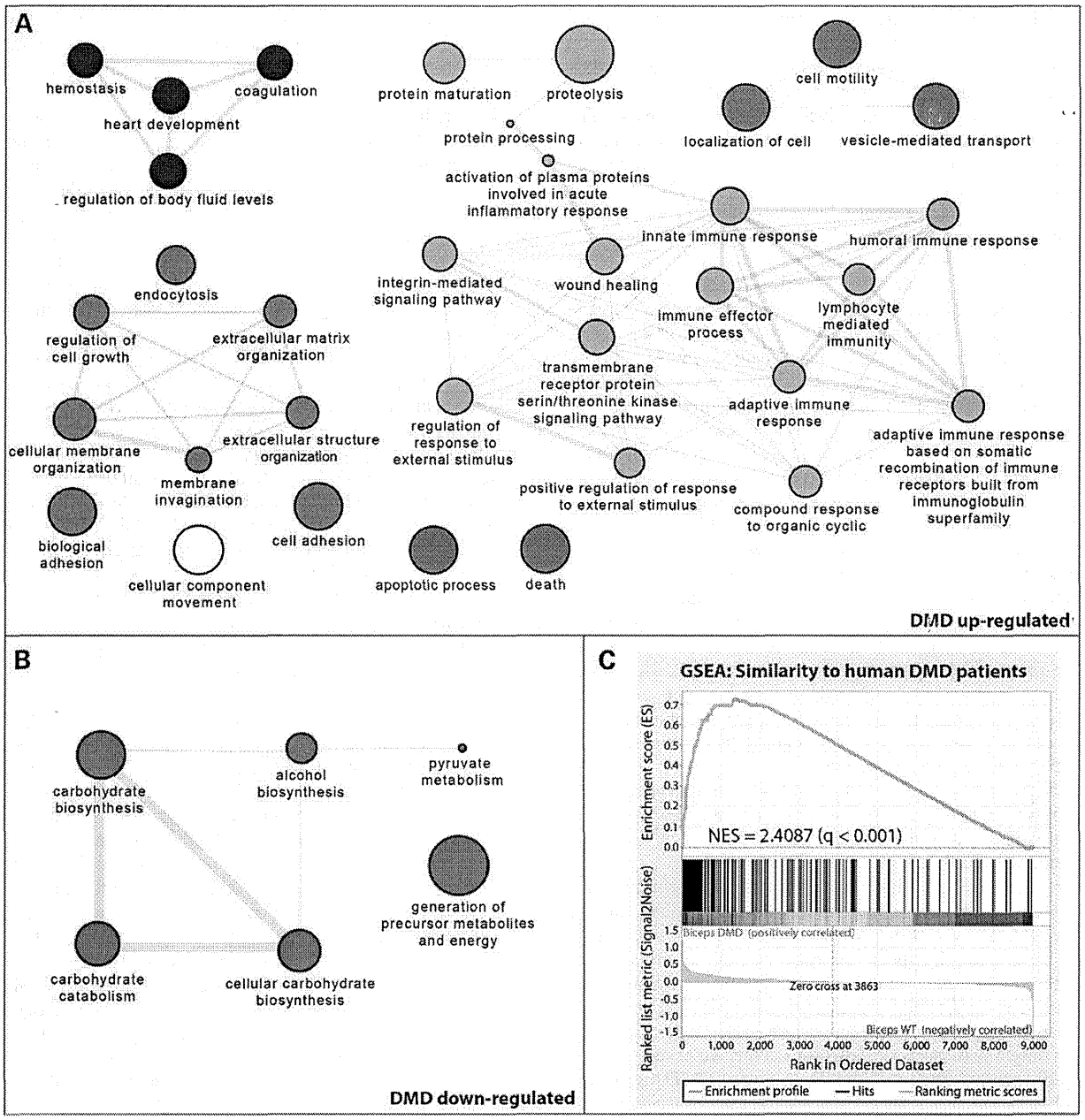

Figure 7. Graph-based visualization of enriched GO terms of genes differentially expressed between DMD and WT pigs at the age of 3 months, and comparison with a transcriptome study of DMD patients. (**A**) GO terms of up-regulated and (**B**) GO terms of down-regulated genes in DMD versus WT pigs. The graphs were produced from all significantly enriched GO terms found by DAVID functional annotation clustering using the tools REVIGO (23) and Cytoscape (24) as explained in legend of Figure 6. (**C**) Gene set enrichment analysis of DEGs up-regulated in 3-month-old DMD pigs versus age-matched WT pigs in a set of genes up-regulated in skeletal muscle of DMD boys younger than 2 years (25). The enrichment profile (green curve) shows a non-random distribution indicated by a roughly triangular outline and a peak close to one of the extremes of the signal-to-noise ordered data set. This distribution means that a higher proportion than expected under the null hypothesis of the genes up-regulated in DMD boys is up-regulated in DMD pigs and fewer than expected are down-regulated or neutral. The leading edge subset containing the most up-regulated genes are the genes positioned left of the peak in the enrichment curve profile. The NES was calculated as outlined in the Materials and Methods section. The q-value is the false discovery rate (FDR) corrected P-value.

the pig (34), demonstrating that BAC targeting and selection of single clones do not interfere with the potential of donor cells to yield cloned offspring.

Pigs lacking *DMD* exon 52 displayed a complete loss of dystrophin, as it is the case in the majority of DMD patients (17). In addition, the levels of dystrophin-associated glycoproteins

α-sarcoglycan and β-dystroglycan were reduced, mirroring the situation in DMD patients.

The DMD pig appears to be a bona fide model of the human dystrophy as ascertained by the absence of the dystrophin protein, elevated serum CK and progressive muscular dystrophy. The percentage of muscle fibre cross-sections with central nuclei (~10%) in 3-month-old DMD pigs appeared rather low when compared with *mdx* mice of the same age (~60%) (35). This might on the one hand reflect a lower regenerative potential of porcine DMD muscles, and might contribute to the accelerated severe muscle phenotype seen in DMD pigs when compared with *mdx* mice. On the other hand, the low percentage of muscle fibres with central nuclei might reflect the young age of the investigated pigs. Likewise, studies in *mdx* mice show that the percentage of muscle fibres with central nuclei increases with age (36). Another important point is that in *mdx* mouse muscle the myonuclei remain central for a long time after regeneration and can thus be used as a marker for regenerated muscle fibres, while in larger mammals the majority of nuclei in regenerating muscle fibres quickly become subsarcolemmal (reviewed in 37). Thus the higher percentage of central nuclei in the *mdx* mouse when compared with the DMD pig may reflect the difference in post-regenerative remodelling in the two species.

In addition to progressive muscle pathology, DMD pigs show characteristic disturbances of locomotion, including the inability in climbing a platform, which is comparable with the early difficulties of DMD patients in climbing stairs. It appears that DMD pigs exhibit the pathological and functional hallmarks of the human disease, but develop them in an accelerated mode. This offers improved opportunities for early and clear-cut read-outs in efficacy studies of new treatments when compared with currently available animal models.

Our findings raise the questions (i) why disease progression in DMD pigs is markedly accelerated when compared with human patients; and (ii) why the severity of muscular dystrophy was associated with birth weight of DMD pigs.

Up-regulation of utrophin at the sarcolemma is a common observation in dystrophin-deficient human and mouse muscle (reviewed in 20). Functional compensation of dystrophin deficiency by utrophin has been demonstrated by amelioration of the pathology in *mdx* mice expressing utrophin transgenes (38,39) and by the fact that double mutant mice lacking both dystrophin and utrophin present a more severe phenotype than mice lacking only one of these proteins (40). Thus we asked whether the rapidly progressing muscular dystrophy of DMD pigs is due to a lack of sarcolemmal utrophin up-regulation. Since increased levels of utrophin have been observed in regenerating, dystrophin-deficient, or inflamed muscle without a corresponding increase in *UTRN* mRNA (41), we compared utrophin expression between DMD and WT pigs on the protein level by western blot and immunohistochemistry. While in muscle specimens of 3-month-old pigs, the sarcolemma stained clearly positive for utrophin, we did not detect sarcolemmal utrophin expression in 2-day-old DMD pigs. The utrophin expression pattern in DMD pigs reflects the situation in humans where young cases of DMD show very little sarcolemmal utrophin, but as the disease progresses utrophin is detectable on many mature muscle fibres (reviewed in 42).

Consistent with these findings, sarcolemmal utrophin was markedly increased in canine X-linked muscular dystrophy (CXMD) in skeletal muscle of 30- and 60-day-old and adult dystrophic animals (43). Moreover, in these dogs, utrophin expression was more persistent when compared with controls and female carriers. In the Golden Retriever muscular dystrophy (GRMD) animal model, a high mortality rate was observed during the first 2 weeks of life (44). Notably, utrophin immunostaining was absent, faintly or variably positive in skeletal muscle from 2-day-old dystrophic CXMD animals which died spontaneously. Similarly absent or variable utrophin expression was reported in puppies which died after days 8, 9 and 11 (43). In line with the findings in neonates of the canine muscular dystrophy model, the lack of sarcolemmal utrophin up-regulation in the 2-day-old DMD pig muscle may contribute to the lethality of some animals shortly after birth.

To gain insight into the hierarchy of disease mechanisms of muscular dystrophy of DMD pigs, we performed a holistic transcriptome analysis of skeletal muscle specimens from 2-day-old and 3-month-old animals. The muscle transcriptome changes of 3-month-old DMD pigs were very similar to those reported for muscle samples of DMD patients, demonstrating that the DMD pig reflects the human disease on the molecular level. In contrast, the transcriptome profile of skeletal muscle from 2-day-old DMD pigs was rather different from published transcriptome data sets of human DMD muscle. Interestingly, *CCL2*—coding for CC chemokine ligand 2, a ligand of CC chemokine receptor 2 (CCR2)—was one of the most down-regulated transcripts in 2-day-old DMD pigs. Experiments in *Ccl2* knockout mice demonstrated that CCL2 deficiency results in reduced inflammation and impaired regeneration after acute muscle injury (45). Further, $Ccl2^{-/-}$ mice exhibited reduced expression of *Igf1*, which was also seen in 2-day-old DMD pigs. In contrast, *CCL2* transcript levels were elevated in 3-month-old versus 2-day-old DMD pigs associated with marked inflammatory and regenerative processes. Thus *CCL2* is an interesting candidate to be involved in the transition from the early lesions observed in 2-day-old DMD piglets to the severe muscular dystrophy observed in 3-month-old DMD pigs with all clinical and pathological hallmarks of human DMD.

A classical hypothesis regarding the pathophysiology of dystrophin deficiency is that abnormal fragility and leakiness of the muscle cell membrane represents the initial pathology of DMD, which is made worse by mechanical stress (reviewed in 20). A primary role of mechanical stress in early DMD pathology is supported by the fact that the set of transcripts with increased abundance in 2-day-old DMD piglets was similar to a set of genes up-regulated in muscle after acute exercise injury (29,30). Our observation that the survival time of DMD pigs was inversely associated with birth weight (Fig. 2A) points to an effect of intrauterine and postnatal growth rate on the severity of the disease. Human foetal growth reaches a maximum between 30 and 36 weeks and declines thereafter as the mother fails to meet the increasing energy demand of her growing foetus. In contrast, pig foetuses have not reached their peak growth rate at birth and can double their birth weight within 7–10 days due to high rates of protein deposition and lean tissue growth and a marked increase in body fat, while human babies need 5 months to double their birth weight (reviewed in 46). Thus, the pig is a model of accelerated growth, which may aggravate the phenotypic consequences of DMD deficiency via different routes. Foetal pig muscles grow by hypertrophy from around day 75 of pregnancy (47). Since